Contents

Introduction

In this work we propose to study the motion of an incompressible two-phase flow. This kind of flows are widely present in our daily life and are of great interest both from a research and an industrial point of view. The main aim of this project is to compare different techniques classically employed in order to solve this complex problem.

We begin by reviewing the governing equations in the first section, then we present the weak formulation associated with the problem and immediately later the algorithms for the numerical approximation.
Finally we apply what we presented in the previous sections to two classical test-cases: the Rayleigh-Taylor instability and the rising bubble.
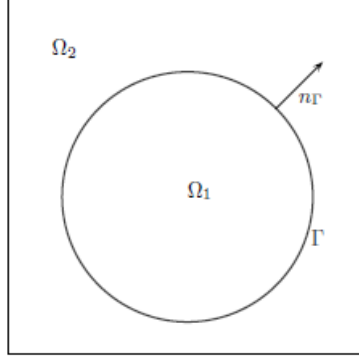
1 Incompressible Two-Phase Flow

Figure 1: Gas bubble in liquid

Let $\Omega \subset \mathbb{R}^2$ be a connected open set and denote by $\boldsymbol{x}$ the spatial coordinates and by t the temporal coordinate. The two fluids in Ω are considered immiscible and they are contained in the subdomains $\Omega_1(t)$ and $\Omega_2(t)$, so that

$$\overline{\Omega_1(t)} \cup \overline{\Omega_2(t)} = \overline{\Omega}$$

The moving interface between the two fluids is denoted by $\Gamma(t)$, defined as:

$$\Gamma(t) := \partial\Omega_1(t) \cap \partial\Omega_2(t)$$

In order to fix the notation, we consider the lighter fluid contained in $\Omega_1(t)$, while the heavier one is inside $\Omega_2(t)$.

1.1 Mathematical model

The governing equations for the fluid motion are the isothermal, incompressible Navier-Stokes equations with gravity, that read as follows:

$$\begin{cases} \rho\left(\frac{\partial \boldsymbol{u}}{\partial t} + (\boldsymbol{u} \cdot \nabla)\,\boldsymbol{u}\right) - \nabla \cdot (2\mu \boldsymbol{D}\,(\boldsymbol{u})) + \nabla p = \rho \boldsymbol{g} & \text{in } \Omega \times (0, T_f) \\ \nabla \cdot \boldsymbol{u} = 0 & \text{in } \Omega \times (0, T_f) \end{cases} \tag{1}$$

Herein ρ denotes the density of the fluid, μ is the dynamic viscosity, $\boldsymbol{u}$ is the velocity of the fluid and p is the pressure.
Moreover $\boldsymbol{g}$ denotes the acceleration of gravity and $\boldsymbol{D}(\boldsymbol{u})$ is the symmetric part of the velocity gradient tensor, namely

$$\boldsymbol{D}(\boldsymbol{u}) = \frac{1}{2}\left(\nabla \boldsymbol{u} + (\nabla \boldsymbol{u})^T\right)$$

T_f is the final time chosen for the problem, ∇ denotes the gradient operator while $\nabla \cdot$ is the divergence operator.

3

The unknowns are the velocity $\boldsymbol{u}$ (more precisely, each $\boldsymbol{u}_i = \boldsymbol{u}|_{\Omega_i}$ is the velocity of the fluid i, $i = 1, 2$) and the pressure p.

We notice immediately that both the density and the viscosity are discontinuous functions

$$\rho = \begin{cases} \rho_1 & \text{in } \Omega_1(t) \\ \rho_2 & \text{in } \Omega_2(t) \end{cases} \qquad \text{and} \qquad \mu = \begin{cases} \mu_1 & \text{in } \Omega_1(t) \\ \mu_2 & \text{in } \Omega_2(t) \end{cases}$$

with $\rho_1 < \rho_2$.

Surface tension effects are taken into accounts through the following balance of forces

$$\begin{cases} [\boldsymbol{u}] = 0 & \text{on } \Gamma(t) \\ [\boldsymbol{T}\boldsymbol{n}_\Gamma] = -\sigma \kappa \boldsymbol{n}_\Gamma & \text{on } \Gamma(t) \end{cases} \tag{2}$$

where $[\cdot]$ is the jump operator, $\boldsymbol{n}_\Gamma$ is the outward unit normal to $\Gamma(t)$, $\boldsymbol{T} = -p\boldsymbol{I} + 2\mu \boldsymbol{D}(\boldsymbol{u})$ is the stress tensor, σ is the surface tension coefficient and $\kappa = \nabla \cdot \boldsymbol{n}_\Gamma$ is the curvature. Finally, we assume that the interface is advected by the velocity of the fluid, namely

$$V_\Gamma = \boldsymbol{u} \cdot \boldsymbol{n}_\Gamma \tag{3}$$

Since the interface is moving, it is convenient to express the surface tension effect through a volumetric force and to include it into the equation (1); define:

$$\boldsymbol{f}_\sigma = -\sigma \kappa \boldsymbol{n}_\Gamma \delta(\Gamma(t))$$

with $\delta(\cdot)$ denoting the Dirac delta. Therefore (1) becomes

$$\begin{cases} \rho \left(\frac{\partial \boldsymbol{u}}{\partial t} + (\boldsymbol{u} \cdot \nabla) \boldsymbol{u} \right) - \nabla \cdot (2\mu \boldsymbol{D}(\boldsymbol{u})) + \nabla p = \rho \boldsymbol{g} + \boldsymbol{f}_\sigma & \text{in } \Omega \times (0, T_f) \\ \nabla \cdot \boldsymbol{u} = 0 & \text{in } \Omega \times (0, T_f) \end{cases} \tag{4}$$

We notice that it is possible to express the term $\boldsymbol{f}_\sigma$ in divergence form; indeed as reported in [5]:

$$\nabla \cdot \Big((\boldsymbol{I} - \boldsymbol{n}_\Gamma \otimes \boldsymbol{n}_\Gamma) \, \delta(\Gamma) \Big) = \nabla_{\text{s}} \cdot (\boldsymbol{I} - \boldsymbol{n}_\Gamma \otimes \boldsymbol{n}_\Gamma) \, \delta(\Gamma) + (\boldsymbol{I} - \boldsymbol{n} \otimes \boldsymbol{n}) \, \nabla \delta(\Gamma) \tag{5}$$

where we omit the explicit dependence of Γ on t and $\nabla_{\text{s}} \cdot$ is the divergence surface operator, defined for a generic function f as follows:

$$\frac{\partial_s f}{\partial x_j} = \frac{\partial \widetilde{f}}{\partial x_j} - \left(\nabla \widetilde{f} \cdot \boldsymbol{n}_\Gamma \right) n_{\Gamma_j}$$

with $\widetilde{f}$ any smooth extension of f outside Γ. Therefore in components we obtain:

$$\begin{aligned}
\left[\nabla_{\text{s}} \cdot (\boldsymbol{I} - \boldsymbol{n}_\Gamma \otimes \boldsymbol{n}_\Gamma) \right]_i &= \frac{\partial \left(\delta_{ij} - n_{\Gamma_i} n_{\Gamma_j} \right)}{\partial x_j} - n_{\Gamma_j} \left(\frac{\partial \left(\delta_{ij} - n_{\Gamma_i} n_{\Gamma_j} \right)}{\partial x_k} \right) n_{\Gamma_k} \\
&= -\frac{\partial n_{\Gamma_i}}{\partial x_j} n_{\Gamma_j} - \frac{\partial n_{\Gamma_j}}{\partial x_j} n_{\Gamma_i} - n_{\Gamma_j} \left(-\frac{\partial n_{\Gamma_i}}{\partial x_k} n_{\Gamma_j} n_{\Gamma_k} - \frac{\partial n_{\Gamma_j}}{\partial x_k} n_{\Gamma_i} n_{\Gamma_k} \right) \\
&= -\frac{\partial n_{\Gamma_i}}{\partial x_j} n_{\Gamma_j} - \frac{\partial n_{\Gamma_j}}{\partial x_j} n_{\Gamma_i} + \frac{\partial n_{\Gamma_i}}{\partial x_k} n_{\Gamma_k} + n_{\Gamma_j} \frac{\partial n_{\Gamma_j}}{\partial x_k} n_{\Gamma_i} n_{\Gamma_k}
\end{aligned}$$

where δ_{ij} is the Kronecker delta and we exploited the fact that $\boldsymbol{n}_\Gamma \cdot \boldsymbol{n}_\Gamma = 1$ in the third term.

At this point we notice that indices can be renamed in the third term and therefore it simplifies with the first one; moreover the last term is equal to zero because

$$2\boldsymbol{n}_\Gamma \cdot \frac{\partial \boldsymbol{n}_\Gamma}{\partial \cdot} = \frac{\partial\,(\boldsymbol{n}_\Gamma \cdot \boldsymbol{n}_\Gamma)}{\partial \cdot} = \frac{\partial 1}{\partial \cdot} = 0$$

Therefore we obtain

$$[\nabla_{\mathrm{s}}\cdot\,(\boldsymbol{I} - \boldsymbol{n}_\Gamma \otimes \boldsymbol{n}_\Gamma)]_i = -\frac{\partial n_{\Gamma_j}}{\partial x_j} n_{\Gamma_i}$$

which in tensorial form means that

$$\nabla_{\mathrm{s}}\cdot\,(\boldsymbol{I} - \boldsymbol{n}_\Gamma \otimes \boldsymbol{n}_\Gamma) = -\,(\nabla\cdot \boldsymbol{n}_\Gamma)\,\boldsymbol{n}_\Gamma$$

If we substitute into we obtain:

$$\nabla\cdot\Big(\,(\boldsymbol{I} - \boldsymbol{n}_\Gamma \otimes \boldsymbol{n}_\Gamma)\,\delta(\Gamma)\Big) = -\,(\nabla\cdot \boldsymbol{n}_\Gamma)\,\boldsymbol{n}_\Gamma\delta(\Gamma) + (\boldsymbol{I} - \boldsymbol{n} \otimes \boldsymbol{n})\,\nabla\delta(\Sigma)$$

Now we refer to [4] and we notice that $\nabla\delta(\Gamma) = (\nabla\delta(\Gamma) \cdot \boldsymbol{n}_\Gamma)\,\boldsymbol{n}_\Gamma$ and therefore:

$$(\boldsymbol{I} - \boldsymbol{n} \otimes \boldsymbol{n})\,\nabla\delta(\Gamma) = (\nabla\delta(\Sigma) \cdot \boldsymbol{n}_\Gamma)\,(\boldsymbol{I} - \boldsymbol{n} \otimes \boldsymbol{n})\,\boldsymbol{n}_\Gamma = \boldsymbol{0}$$

since $(\boldsymbol{n}_\Gamma \otimes \boldsymbol{n}_\Gamma)\,\boldsymbol{n}_\Gamma = \boldsymbol{n}_\Gamma$. Hence we end up with the following equivalent relation for the volumetric force $\boldsymbol{f}_\sigma$:

$$\boldsymbol{f}_\sigma = -\sigma\,(\nabla\cdot \boldsymbol{n}_\Gamma)\,\boldsymbol{n}_\Gamma\delta(\Gamma(t)) = \sigma\,\nabla\cdot\Big(\,(\boldsymbol{I} - \boldsymbol{n}_\Gamma \otimes \boldsymbol{n}_\Gamma)\,\delta(\Gamma(t))\Big) \tag{6}$$

A level-set approach is employed to describe the interface $\Gamma(t)$.

Let φ be a signed distance function to $\Gamma(t)$; in particular we define:

$$\varphi(\boldsymbol{x}, t) = \begin{cases} -\mathrm{dist}(\boldsymbol{x}, \Gamma(t)) & \text{if } \boldsymbol{x} \in \Omega_1(t) \\ 0 & \text{if } \boldsymbol{x} \in \Gamma(t) \\ \mathrm{dist}(\boldsymbol{x}, \Gamma(t)) & \text{if } \boldsymbol{x} \in \Omega_2(t) \end{cases}$$

where

$$\mathrm{dist}(\boldsymbol{x}, \Gamma(t)) = \inf_{\boldsymbol{y} \in \Gamma(t)} \mathrm{dist}(\boldsymbol{x}, \boldsymbol{y})$$

Due to its definition the following property holds:

$$\Gamma(t) = \big\{\boldsymbol{x} \in \overline{\Omega} : \varphi\,(\boldsymbol{x}, t) = 0\big\}$$

Thanks to hypothesis (3), the equation that characterizes the level-set method is the following:

$$\frac{\partial \varphi}{\partial t} + \boldsymbol{u} \cdot \nabla\varphi = 0 \qquad \text{in } \Omega \times (0, T_f) \tag{7}$$

5

The previous relation can be further justified as it follows: let $\overline{\boldsymbol{x}}(t)$ be the path of a point on the interface $\Gamma(t)$; this point is moving with the fluid and therefore

$$\frac{d\overline{\boldsymbol{x}}(t)}{dt} = \boldsymbol{u}(\overline{\boldsymbol{x}}(t), t)$$

At this point we notice that the function φ is identically equally to 0 on the moving interface, which means

$$\varphi(\overline{\boldsymbol{x}}(t), t) = 0$$

Taking the total derivative of the above relation we immediately obtain:

$$\frac{\partial\varphi}{\partial t} + \boldsymbol{u} \cdot \nabla\varphi = 0 \qquad \text{in } \Gamma(t) \times (0, T_f) \tag{8}$$

In order to extend the previous relation to the whole domain, as stated in (7), we consider the path of a generic point and we impose the condition that the sign of $\varphi(\overline{\boldsymbol{x}}(t), t)$ does not change:

$$\varphi(\overline{\boldsymbol{x}}(t), t) = \pm c$$

with $c > 0$ and $\varphi(\overline{\boldsymbol{x}}(t), t) < 0$ in Ω_1; in this way $\overline{\boldsymbol{x}}(t)$ belongs to the corresponding sub-domain for all the time.

Since we picked φ such that $\varphi(\boldsymbol{x}, t) < 0$ if $\boldsymbol{x} \in \Omega_1$ and $\varphi(\boldsymbol{x}, t) > 0$ if $\boldsymbol{x} \in \Omega_2$, the following relation holds:

$$\boldsymbol{n}_\Gamma = \frac{\nabla\varphi}{|\nabla\varphi|} \tag{9}$$

and moreover we can express the density and the dynamic viscosity through the Heaviside function H:

$$\rho = \rho_1 + (\rho_2 - \rho_1) H(\varphi) \tag{10}$$

$$\mu = \mu_1 + (\mu_2 - \mu_1) H(\varphi) \tag{11}$$

It is also simple to check that (7) implies mass conservation, at least from an analytical point of view:

$$\frac{\partial\rho}{\partial t} + \boldsymbol{u} \cdot \nabla\rho = (\rho_2 - \rho_1) \left(\frac{\partial H(\varphi)}{\partial t} + \boldsymbol{u} \cdot \nabla H(\varphi) \right)$$

$$= (\rho_2 - \rho_1) \delta(\varphi) \left(\frac{\partial\varphi}{\partial t} + \boldsymbol{u} \cdot \nabla\varphi \right) = 0$$

Finally for density, viscosity and the surface tension term we apply the so called Continuum Surface Force (CSF) approach developed in [8]; we introduce the following smooth regularization of the Heaviside function for a (small) $\varepsilon > 0$

$$H_\varepsilon(\psi) = \begin{cases} 0 & \text{if } \psi < -\varepsilon \\ \frac{1}{2}\left(1 + \frac{\psi}{\varepsilon} + \frac{1}{\pi}\sin\left(\frac{\pi\psi}{\varepsilon}\right)\right) & \text{if } |\psi| \leq \varepsilon \\ 1 & \text{if } \psi > \varepsilon \end{cases}$$

One important thing has to be pointed out at this stage: as reported in [4] the relation between the Dirac delta localized on the interface $\delta(\Gamma)$ and the one localized on the function φ which implicitly describes the surface $\delta(\varphi)$ is the following:

$$\delta(\Gamma) = \delta(\varphi)\,|\nabla\varphi| \tag{12}$$

Therefore $\delta(\varphi)$ is approximated through $\delta_\varepsilon(\varphi) = \frac{dH_\varepsilon(\varphi)}{d\varphi}$ with:

$$\delta_\varepsilon(\psi) = \begin{cases} 0 & \text{if } |\psi| > \varepsilon \\ \frac{1}{2\varepsilon}\left(1 + \cos\left(\frac{\pi\psi}{\varepsilon}\right)\right) & \text{if } |\psi| \leq \varepsilon \end{cases}$$

Hence we rewrite:

$$\rho = \rho_1 + (\rho_2 - \rho_1)\,H_\varepsilon(\varphi) \tag{13}$$

$$\mu = \mu_1 + (\mu_2 - \mu_1)\,H_\varepsilon(\varphi) \tag{14}$$

$$\boldsymbol{f}_\sigma = -\sigma\,(\nabla\cdot\boldsymbol{n}_\Gamma)\,\boldsymbol{n}_\Gamma\delta_\varepsilon(\varphi)\,|\nabla\varphi| = \sigma\,\nabla\cdot\left(\left(\boldsymbol{I} - \boldsymbol{n}_\Gamma \otimes \boldsymbol{n}_\Gamma\right)\delta_\varepsilon(\varphi)\,|\nabla\varphi|\right) \tag{15}$$

1.2 Dimensional analysis

Before computing the variational formulation, a good practice is to derive the non-dimensional version of the Navier-Stokes equations in order to identify the dominant terms in the equation. This procedure can be introduced by scaling the length and the velocity with two characteristic parameters, respectively L and U:

$$\boldsymbol{x} = L\boldsymbol{x}^* \qquad \boldsymbol{u} = U\boldsymbol{u}^* \qquad t = \frac{L}{U}t^*$$

Moreover we choose here as reference density and viscosity the ones associated to the heavier fluid and therefore we obtain:

$$\rho = \rho_2\rho^* \qquad \mu = \mu_2\mu^* \qquad p = \rho_2 U^2 p^* \qquad k = \frac{1}{L}k^*$$

Applying the adimensionalization procedure we obtain:

$$\rho_2\frac{U^2}{L}\rho^*\left(\frac{\partial\boldsymbol{u}^*}{\partial t} + (\boldsymbol{u}^* \cdot \nabla^*)\,\boldsymbol{u}^*\right) - \mu_2\frac{U}{L^2}\nabla\cdot^*(2\mu^*\boldsymbol{D}^*(\boldsymbol{u}^*)) + \rho_2\frac{U^2}{L}\nabla^*p^* = \rho_2\rho^*\boldsymbol{g} - \frac{1}{L^2}\sigma\kappa^*\boldsymbol{n}_\Gamma\delta(\Gamma)$$

which reduces to:

$$\rho^*\left(\frac{\partial\boldsymbol{u}^*}{\partial t} + (\boldsymbol{u}^* \cdot \nabla^*)\,\boldsymbol{u}^*\right) - \frac{1}{Re}\nabla\cdot^*(2\mu^*\boldsymbol{D}^*(\boldsymbol{u}^*)) + \nabla^*p^* = -\frac{1}{Fr^2}\rho^*\boldsymbol{e}_2 - \frac{1}{We}\sigma\kappa^*\boldsymbol{n}_\Gamma\delta(\Gamma)$$

where

$$Re = \frac{\rho_2 UL}{\mu_2} \qquad Fr = \sqrt{\frac{U^2}{gL}} \qquad We = \frac{\rho_2 U^2 L}{\sigma}$$

7

are respectively the Reynolds, the Froude number and the Weber number [22], whereas $e_2 = (0, 1)$ is the unit vector along the vertical direction.

From now on we omit the symbol $(\cdot)^*$ to denote adimensional quantities and therefore we obtain the following equation:

$$\rho \left(\frac{\partial \boldsymbol{u}}{\partial t} + (\boldsymbol{u} \cdot \nabla) \boldsymbol{u} \right) - \frac{1}{Re} \nabla \cdot (2\mu \boldsymbol{D}(\boldsymbol{u})) + \nabla p = -\frac{1}{Fr^2} \rho \boldsymbol{e}_2 - \frac{1}{We} \sigma \kappa \boldsymbol{n}_\Gamma \delta(\Gamma) \qquad (16)$$

It is simple to check that the other two equations, namely the divergence-free constraint and the advection of level set function, preserve the same structure also in non-dimensional form.

1.3 Reinitialization

A signed distance function satisfies

$$|\nabla \varphi| = 1$$

also known as Eikonal equation as reported in [20]. This is the main reason for which φ has been taken in this way: indeed, as explained in [18], flat gradients can cause numerical instabilities and loss in accuracy, while large gradients produce larger errors. As the level set is transported it will change its shape during the computations and therefore it will lose the look that we desire, namely being a signed distance function. The term employed to describe the process of updating the level set function φ in order to preserve its peculiarities as much as possible is *reinitialization*.

As reported in [19], a common approach for this step has been proposed by Sussman et al. [9] and it is based on the steady-state of a PDE

$$\frac{\partial \varphi}{\partial \tau} - \text{sgn}(\varphi_0) \left(1 - |\nabla \varphi|^2 \right) = 0 \qquad (17)$$

where φ_0 is the current level set function obtain after the advection step and τ represents a pseudo-time different from the one used in the Navier-Stokes equations and in the level-set method. The sign function is approximated by a smooth function

$$\text{sgn}_\gamma(\varphi_0) = \frac{\varphi_0}{\sqrt{\varphi_0^2 + \gamma^2 |\nabla \varphi_0|^2}} \qquad (18)$$

with γ small parameter that prevents discontinuous transition.

However, as reported in [18], this PDE is not very stable from a numerical point of view because of its high non-linearity and therefore measures to improve stability must be taken by introducing an artificial diffusion term:

$$\frac{\partial \varphi}{\partial \tau} - \text{sgn}_\gamma(\varphi_0) \left(1 - |\nabla \varphi|^2 \right) - \beta \nabla^2 \varphi = 0 \qquad (19)$$

1.4 Conservative level-set method

The standard level-set method has some drawbacks and in particular it lacks of mass conservation. This problem is further emphasized by the reinizialization procedure introduced above since the interface may move a little during the process in case φ is not smooth or is much steeper on one side of the interface than the other [11].
As reported in [19], Olsson and Kreiss [12] proposed a conservative level-set method. The idea of the scheme is to replace the signed distance function introduced above with a 'regularized' Heaviside function:

$$\phi(\boldsymbol{x},t) = \frac{1}{1 + e^{-\varphi(\boldsymbol{x},t)/\varepsilon}} \tag{20}$$

where ε helps smoothing the transition of the discontinuous physical properties between the two sub-domains; it is also called *interface thickness*. Since

$$\nabla\phi = \frac{1}{\varepsilon}\frac{e^{-\varphi/\varepsilon}}{\left(1 + e^{-\varphi/\varepsilon}\right)^2}\nabla\varphi$$

we can compute the outward unit normal $\boldsymbol{n}_\Gamma$ exactly as in (9) and therefore

$$\boldsymbol{n}_\Gamma = \frac{\nabla\phi}{|\nabla\phi|} \tag{21}$$

From the definition of $\phi(\boldsymbol{x},t)$ it follows immediately that

$$\Gamma(t) := \left\{\boldsymbol{x} \in \overline{\Omega} : \phi(\boldsymbol{x},t) = \frac{1}{2}\right\} \tag{22}$$

This new level set function needs anyway to be reinitialized in order to keep the property of being a regularized Heaviside function. The approach chosen for this step is the one proposed in [15] which is still based on the steady-state of a PDE and reads as follows:

$$\frac{\partial\phi}{\partial\tau} + \nabla\cdot\left(\phi\left(1 - \phi\right)\boldsymbol{n}_\Gamma\right) = \varepsilon\,\nabla\cdot\left(\left(\nabla\phi\cdot\boldsymbol{n}_\Gamma\right)\boldsymbol{n}_\Gamma\right) \tag{23}$$

with τ pseudo time-step exactly like in the previous reinitialization algorithm.

It is important to notice that (23) is expressed in conservative form and that $\boldsymbol{n}_\Gamma$ does not change during the reinizialization procedure, but is computed using the initial value of the level set function after the transport.

Finally, we stress the fact that, in this method, we are already using a smooth version of Heaviside function and therefore

$$H_\varepsilon = \phi \tag{24}$$

$$\delta(\Gamma) \approx \frac{dH_\varepsilon}{d\phi}\,|\nabla\phi| = |\nabla\phi| \tag{25}$$

2 Variational formulation

In order to complete the definition of the problem we need to assign appropriate initial and boundary conditions.

We assume that the initial velocity $\boldsymbol{u}_0$ and the initial location of the interface $\Gamma(0)$ are known; moreover we denote by $\partial\Omega_D$ the portion of $\partial\Omega$ where we impose Dirichlet boundary conditions, namely $\boldsymbol{u} = \boldsymbol{u}_D$ on $\partial\Omega_D$ and we impose homogeneous natural boundary conditions on $\partial\Omega \setminus \partial\Omega_D$:

$$-p\boldsymbol{n} + 2\mu\boldsymbol{D}(\boldsymbol{u})\boldsymbol{n} = \boldsymbol{0} \qquad \text{on } \partial\Omega \setminus \partial\Omega_D$$

where $\boldsymbol{n}$ denotes the generic outward unit normal from the boundary.

We seek now a suitable weak formulation; in order to derive it we introduce the following spaces

$$\begin{aligned}
\boldsymbol{V} &= \left[\boldsymbol{H}^1(\Omega)\right]^2 \\
\boldsymbol{V}_D &= \{\boldsymbol{v} \in \boldsymbol{V} : \boldsymbol{v} = \boldsymbol{0} \text{ on } \partial\Omega_D\} \\
Q &= L^2(\Omega) \\
Z &= H^1(\Omega)
\end{aligned}$$

Moreover, for a generic Banach space W equipped with the norm $\|\cdot\|_W$ we introduce the following spaces:

$$L^2(0, T_f; W) = \left\{f : (0, T_f) \to W : t \to f(t) \text{ is measurable and } \int_0^{T_f} \|f(t)\|_W < +\infty\right\}$$

$$L^\infty(0, T_f; W) = \{f : (0, T_f) \to W : t \to f(t) \text{ is measurable and } \|f(t)\|_W < +\infty \quad \forall t \in (0, T_f)\}$$

$$C^0(0, T_f; W) = \{f : (0, T_f) \to W : t \to f(t) \text{ is continuous and } \|f(t)\|_W < +\infty \quad \forall t \in (0, T_f)\}$$

Using the representation of the material properties in the whole domain and defining the interface by means of the level-set method, we end up with the following variational formulation:

Find

- $\boldsymbol{u}(t) \in L^2\left(0, T_f; \boldsymbol{V}\right) \bigcap L^\infty\left(0, T_f; \left[L^2(\Omega)\right]^2\right)$

- $p(t) \in L^2\left(0, T_f; Q\right)$

- $\varphi(t) \in C^0\left(0, T_f; Z\right)$

with

- $\boldsymbol{u}(t) = \boldsymbol{u}_D$ on $\partial\Omega_D$, $\boldsymbol{u}(0) = \boldsymbol{u}_0 \in \boldsymbol{V}$ s.t. $\nabla\cdot\boldsymbol{u}_0 = 0$

- $\varphi(0) = \varphi_0 \in Z$

such that for almost all $t \in [0, T_f]$:

$$\int_\Omega \rho \left(\frac{\partial \boldsymbol{u}}{\partial t} + (\boldsymbol{u} \cdot \nabla) \boldsymbol{u} \right) \cdot \boldsymbol{v} d\Omega + \frac{2}{Re} \int_\Omega \mu \boldsymbol{D}(\boldsymbol{u}) : \nabla \boldsymbol{v} d\Omega - \int_\Omega p \, \nabla \cdot \boldsymbol{v} d\Omega$$

$$+ \frac{1}{Fr^2} \int_\Omega \boldsymbol{e}_2 \cdot \boldsymbol{v} d\Omega + \frac{1}{We} \int_\Omega \kappa \boldsymbol{n}_\Gamma \frac{dH_\varepsilon(\varphi)}{d\varphi} \cdot \boldsymbol{v} d\Omega = 0 \qquad \forall \boldsymbol{v} \in \boldsymbol{V}_0 \qquad (26)$$

$$\int_\Omega q \, \nabla \cdot \boldsymbol{u} = 0 \qquad \forall q \in Q \qquad (27)$$

$$\int_\Omega \frac{\partial \varphi}{\partial t} z d\Omega + \int_\Omega (\boldsymbol{u} \cdot \nabla \varphi) z d\Omega = 0 \qquad \forall z \in Z \qquad (28)$$

Herein we denoted by φ the generic level set function independently on the method chosen to solve this step.

Remark In case of a fully Dirichlet problem ($\partial \Omega_D = \partial \Omega$), the pressure is defined up to an arbitrary constant since it appears in the equation only under derivative operator and is not fixed by any boundary condition; in this situation the space Q is typically replaced by

$$Q = L_0^2(\Omega) = \left\{ q \in L^2(\Omega) : \int_\Omega q d\Omega = 0 \right\}$$

which is the space of square integrable functions with zero average.

Let us briefly analyze (26); in this relation the symbol : denotes the inner product between two second-order tensors, defined as follows:

$$\boldsymbol{A} : \boldsymbol{B} = A_{ij} B_{ij}$$

where the Einstein notation, namely repeated indices are intended to be summed up, is employed.
The relation (26) can be further simplified; indeed since every second-order tensor can be expressed as the sum of a symmetric and a skew-symmetric second-order tensor and the inner product between a symmetric and a skew-symmetric tensor is 0, we immediately obtain:

$$\boldsymbol{D}(\boldsymbol{u}) : \nabla \boldsymbol{v} = \boldsymbol{D}(\boldsymbol{u}) : \boldsymbol{D}(\boldsymbol{v})$$

Moreover thanks to (6) we can rewrite

$$\frac{1}{We} \int_\Omega \kappa \boldsymbol{n}_\Gamma \frac{dH_\varepsilon(\varphi)}{d\varphi} \cdot \boldsymbol{v} d\Omega = -\frac{1}{We} \int_\Omega \nabla \cdot \left((\boldsymbol{I} - \boldsymbol{n}_\Gamma \otimes \boldsymbol{n}_\Gamma) \frac{dH_\varepsilon(\varphi)}{d\phi} \right) \cdot \boldsymbol{v} d\Omega \qquad (29)$$

Integrating by parts we obtain:

$$- \int_\Omega \nabla \cdot \left((\boldsymbol{I} - \boldsymbol{n}_\Gamma \otimes \boldsymbol{n}_\Gamma) \frac{dH_\varepsilon(\varphi)}{d\phi} \right) \cdot \boldsymbol{v} d\Omega =$$

$$- \int_{\partial \Omega} \left((\boldsymbol{I} - \boldsymbol{n}_\Gamma \otimes \boldsymbol{n}_\Gamma) \frac{dH_\varepsilon(\varphi)}{d\phi} \right) \boldsymbol{n} \cdot \boldsymbol{v} d\Sigma + \int_\Omega \left((\boldsymbol{I} - \boldsymbol{n}_\Gamma \otimes \boldsymbol{n}_\Gamma) \frac{dH_\varepsilon(\varphi)}{d\phi} \right) : \nabla \boldsymbol{v} d\Omega \quad (30)$$

11

Since $\frac{dH_\varepsilon(\varphi)}{d\varphi}$ is an approximation of the Dirac delta localized on the interface, if ε is sufficiently small and if we assume that the interface does not intersect $\partial\Omega$ (or at least $\partial\Omega \setminus \partial\Omega_D$), the contribution due to the boundary integral vanishes. We also notice that, in case of full Dirichlet boundary conditions, the same consideration is valid since $\boldsymbol{v} \in \boldsymbol{V}_0$. Moreover $\boldsymbol{I} - \boldsymbol{n}_\Gamma \otimes \boldsymbol{n}_\Gamma$ is a symmetric tensor and so the following relation holds:

$$(\boldsymbol{I} - \boldsymbol{n}_\Gamma \otimes \boldsymbol{n}_\Gamma) : \nabla \boldsymbol{v} = (\boldsymbol{I} - \boldsymbol{n}_\Gamma \otimes \boldsymbol{n}_\Gamma) : \boldsymbol{D}(\boldsymbol{v})$$

Hence (26) can be rewritten as it follows

$$\int_\Omega \rho \left(\frac{\partial \boldsymbol{u}}{\partial t} + (\boldsymbol{u} \cdot \nabla) \boldsymbol{u} \right) \cdot \boldsymbol{v} d\Omega + \frac{2}{Re} \int_\Omega \mu \boldsymbol{D}(\boldsymbol{u}) : \boldsymbol{D}(\boldsymbol{v}) d\Omega - \int_\Omega p \nabla \cdot \boldsymbol{v} d\Omega$$

$$+ \frac{1}{Fr^2} \int_\Omega \boldsymbol{e}_2 \cdot \boldsymbol{v} d\Omega + \frac{1}{We} \left((\boldsymbol{I} - \boldsymbol{n}_\Gamma \otimes \boldsymbol{n}_\Gamma) \frac{dH_\varepsilon(\varphi)}{d\phi} \right) : \boldsymbol{D}(\boldsymbol{v}) = 0 \qquad \forall \boldsymbol{v} \in \boldsymbol{V}_0 \qquad (31)$$

2.1 Well posedness

The well posedness of the Navier-Stokes equations is a very complex topic of great research interest.

In 2D existence and uniqueness result of the solution has been obtained; before stating this theorem we notice that for our hypotheses about reference density and viscosity

$$\frac{\rho_1}{\rho_2} \leq \rho \leq 1$$

$$\frac{\mu_1}{\mu_2} \leq \mu \leq 1$$

Moreover $\frac{dH_\varepsilon(\varphi)}{d\varphi}$ is uniformly bounded in both configurations considered, namely it is bounded by a constant which does not depend on φ; in particular

$$\frac{dH_\varepsilon}{d\varphi} \leq \frac{1}{\varepsilon}$$

Therefore if $\varphi \in L^4(0, T_f; W^{1,4}(\Omega))$, the quantity $\boldsymbol{f}_\sigma \in L^2(0, T_f; \left[H^{-1}(\Omega) \right]^2)$ where

$$W^{k,p} = \{ f \in L^p(\Omega) : D^\alpha f \in L^p(\Omega) \quad \forall \alpha \leq k \}$$

is a standard Sobolev space and $\left[H^{-1}(\Omega) \right]^2$ is the dual space of $\boldsymbol{V}_0$.

Hence we are ready to state the following theorem:

Theorem 2.1 *If $\varphi \in L^4(0, T_f; W^{1,4}(\Omega))$, the problem (31)-(27) admits a unique solution $(\boldsymbol{u}, p)$ with $\boldsymbol{u} \in L^2\left(0, T_f; \boldsymbol{V}\right) \bigcap L^\infty\left(0, T_f; (L^2(\Omega))^2\right)$ and $p \in L^2\left(0, T_f; L^2(\Omega)\right)$.*

The proof can be found in [3, Chap. V, Thms 1.4 & 1.5]

The level-set method employs instead a hyperbolic equation and only existence results can be proven in general.

Let us consider for a while a simplified case where we keep a sufficiently regular $\boldsymbol{u}$ and $\boldsymbol{u}_D = \boldsymbol{0}$ on $\partial\Omega$ (no-slip condition); more in detail we state the following theorem:

Theorem 2.2 *Assume the function $\boldsymbol{u}$ is divergence-free such that*

$$\boldsymbol{u} \in C^0\left(0, T_f, \boldsymbol{V}_0\right) \bigcap C^0\left(0, T_f, \left[W^{1,\infty}\right]^2\right) \tag{32}$$

Then for any $\varphi_0 \in L^2(\Omega)$ the problem

$$\begin{cases} \frac{\partial \varphi}{\partial t} + \boldsymbol{u} \cdot \nabla \varphi = 0 & in \ \Omega \times (0, T_f) \\ \varphi(\cdot, 0) = \varphi_0 \end{cases}$$

admits a unique solution $\varphi(t) \in C^0\left(0, T_f, L^2(\Omega)\right)$

Proof First of all we prove the existence of a solution. We notice that the equation of our interest can be rewritten as

$$\frac{D\varphi}{Dt} = 0$$

where $\frac{D\cdot}{Dt}$ denotes the total derivative operator; this means that it exists a function $\boldsymbol{X}(\boldsymbol{x}, s; t)$ known as characteristic function such that

$$\frac{d\varphi(\boldsymbol{X}(t), t)}{dt} = 0$$

where

$$\begin{cases} \frac{d\boldsymbol{X}}{dt} = \boldsymbol{u}(\boldsymbol{X}, t) & in \ \Omega \times (0, T_f) \\ \boldsymbol{X}(\boldsymbol{x}, s; x) = \boldsymbol{x} \end{cases}$$

Hence $\boldsymbol{X}$ represents the trajectory of a particle that at time s is in $\boldsymbol{x}$.

Thanks to the property (32) we can apply the Cauchy-Lipschitz theorem and therefore we have the existence of the ordinary differential equation that governs $\boldsymbol{X}$. Thus it follows immediately that the function φ is defined by

$$\varphi(\boldsymbol{x}, t) = \varphi_0(\boldsymbol{X}(\boldsymbol{x}, t))$$

is a solution of our problem.

Now we are ready to prove the uniqueness. Let φ_1 and φ_2 be two solutions of our equation and define $\varphi = \varphi_1 - \varphi_2$. If we multiply the difference of the two equations by φ we obtain:

$$\frac{1}{2}\frac{\partial \varphi^2}{\partial t} + \frac{1}{2}\boldsymbol{u} \cdot \nabla \varphi^2 = 0$$

Since $\boldsymbol{u}$ is divergence-free and $\boldsymbol{u}$ vanishes on the boundary, integrating by parts on Ω we find

$$\frac{1}{2}\frac{d \|\varphi\|^2_{L^2(\Omega)}}{dt} = 0$$

and since $\varphi(\cdot, 0) = 0$ we obtain $\varphi(\cdot, t) = 0 \quad \forall t$ which means that the solution is unique.

From the proof above it is clear that the hypothesis $\boldsymbol{u}_D = \boldsymbol{0}$ on $\partial\Omega$ is not fundamental and it is sufficient $\boldsymbol{u} \cdot \boldsymbol{n} = 0$ on $\partial\Omega$ (free-slip condition) in order to avoid any boundary contribution: for this reason from now on we will move into this framework and we require the additional compatibility condition on initial data, namely

$$\boldsymbol{u}_0 \cdot \boldsymbol{n} = 0 \qquad \text{on } \partial\Omega \tag{33}$$

Moreover the hypotheses on the regularity of $\boldsymbol{u}$ can be relaxed: for further detail please refer to [7, Section IV.4].

Eventually we notice that the regularity of the solution φ depends on the regularity of φ_0 and this is the reason for which we require $\varphi_0 \in H^1(\Omega)$.

2.2   Variational formulation for the reconstruction

The weak formulation of (19) reads as follows:

$$\int_\Omega \frac{\partial\varphi}{\partial\tau} z d\Omega + \int_\Omega \text{sign}_\gamma(\varphi_0) \left(1 - |\nabla\varphi|\right) z d\Omega + \beta \int_\Omega \nabla\varphi \cdot \nabla z d\Omega = 0 \quad \forall z \in Z \tag{34}$$

where here we assume that
$$\nabla\varphi \cdot \boldsymbol{n} = 0 \qquad \text{on } \partial\Omega$$

This hypothesis means that we do not allow a 'flux' of interface along the boundary of the domain Ω, which seems to be reasonable since we have already assumed that the interface does not intersect $\partial\Omega$ and we are only interested in cases for which the interface remains inside the domain Ω.

The same hypothesis is assumed in the case of conservative level-set method; therefore the weak formulation of (23) is:

$$\int_\Omega \frac{\partial\varphi}{\partial\tau} z d\Omega - \int_\Omega (\varphi(1-\varphi)\boldsymbol{n}_\Gamma) \cdot \nabla z d\Omega + \varepsilon \int_\Omega ((\nabla\varphi \cdot \boldsymbol{n}_\Gamma)\boldsymbol{n}_\Gamma) \cdot \nabla z d\Omega = 0 \quad \forall z \in Z \tag{35}$$

All the boundary contributions vanish since under homogeneous Neumann boundary conditions
$$\boldsymbol{n}_\Gamma \cdot \boldsymbol{n} = \frac{\nabla\varphi}{|\nabla\varphi|} \cdot \boldsymbol{n} = 0 \qquad \text{on } \partial\Omega$$

3   Numerical approximation

We are now ready to present the numerical approximation of the problem, based on the finite elements method.

Consider a discretization of Ω into a family of triangulations $\mathcal{T}_h$ and denote by K each element; moreover denote by h_K the diameter of each element K where

$$\text{diam}(K) = \max_{\boldsymbol{x},\boldsymbol{y}\in K} |\boldsymbol{x} - \boldsymbol{y}|$$

and eventually define

$$h = \min_{K\in\mathcal{T}_h} h_K$$

We define a scalar and continuous finite element space as follows:

$$X_h^r = \left\{ v \in C^0(\Omega) : v|_K \in \mathbb{P}_r(K) \quad \forall K \in \mathcal{T}_h \right\}$$

where $\mathbb{P}_r$ is the space of polynomials of degree r. We choose to represent

$$\boldsymbol{u}_h(t) \in \left[X_h^{r+1} \right]^2 = \boldsymbol{V}_h$$
$$p_h(t) \in X_h^r = Q_h$$

where $\boldsymbol{u}_h(t)$ and $p_h(t)$ are the semi-discretized approximations of $\boldsymbol{u}$ and p respectively and $r \geq 1$.

For what concerns $\varphi_h(t)$, the semi-discretization of the level set function, we pick

$$\varphi_h(t) \in X_h^s = Z_h$$

with $s \geq 1$.

The time discretization is simply performed introducing a uniform partition of the interval $[0, T_f]$ with $0 = t_0 < t_1 < t_2 < ... < t_{N-1} < t_N = T_f$ such that the time-step $\Delta t = \frac{T_f}{N}$ and $t_n = n\Delta t$.

Finally we denote by $\boldsymbol{u}_h^n, p_h^n$ and φ_h^n the value of $\boldsymbol{u}_h, p_h$ and φ_h at time t_n.

In our simulations we choose to solve first the level-set method equation using as advection velocity the one of the previous time-step and then we update density and viscosity in order to solve the Navier-Stokes equations.

Hence given $\boldsymbol{u}_h^n, p_h^n, \varphi_h^n$ we compute the triple $(\boldsymbol{u}_h^{n+1}, p_h^{n+1}, \varphi_h^{n+1})$ by solving

$$\int_\Omega \left(\frac{\rho(\varphi_h^{n+1})\boldsymbol{u}_h^{n+1} - \rho(\varphi_h^n)\boldsymbol{u}_h^n}{\Delta t} + (\boldsymbol{u}_h^n \cdot \nabla)\, \boldsymbol{u_h^{n+1}} \right) \cdot \boldsymbol{v}_h d\Omega + \frac{2}{Re} \int_\Omega \mu(\varphi_h^{n+1})\boldsymbol{D}(\boldsymbol{u}_h^{n+1}) : \boldsymbol{D}(\boldsymbol{v}_h)d\Omega -$$

$$\int_\Omega p_h^{n+1} \nabla\cdot\boldsymbol{v}_h d\Omega + \frac{1}{A}\int_\Omega \boldsymbol{e}_2 \cdot \boldsymbol{v}_h d\Omega + \frac{1}{A}\frac{1}{Bo}\int_\Omega (\boldsymbol{I} - \boldsymbol{n}_\Gamma \otimes \boldsymbol{n}_\Gamma)\frac{dH_\varepsilon(\varphi_h^{n+1})}{d\varphi} : D(\boldsymbol{v}_h)d\Omega = 0 \quad \forall \boldsymbol{v}_h \in \boldsymbol{V}_h \quad (36)$$

$$\int_\Omega q_h \nabla\cdot\boldsymbol{u}_h^{n+1} = 0 \qquad \forall q_h \in Q_h \tag{37}$$

$$\int_\Omega \frac{\varphi_h^{n+1} - \varphi_h^n}{\Delta t} z_h d\Omega + \int_\Omega \boldsymbol{u}_h^n \cdot \nabla\varphi_h^{n+1} z_h d\Omega = 0 \qquad \forall z_h \in Z_h \tag{38}$$

We choose here a semi-implicit treatment for the velocity since unconditional stability holds in that case, while the normal $\boldsymbol{n}_\Gamma$ is computed through the formula

$$\boldsymbol{n}_\Gamma = \frac{\nabla \varphi_h}{|\nabla \varphi_h|}$$

Moreover since we expect not to work with high Reynolds numbers we do not add a stabilization term in the Navier-Stokes equations.

For what concerns the boundary conditions we set $\boldsymbol{u}_h^{n+1} = \boldsymbol{u}_{D_h}$ where $\boldsymbol{u}_{D_h}$ is a suitable approximation of $\boldsymbol{u}_D$ in the space $\boldsymbol{V}_h(\partial \Omega_D)$ usually obtained by interpolation or projection, while for the initial conditions we set

$$\boldsymbol{u}_h^0 = \boldsymbol{u}_{0_h}$$
$$\varphi_h^0 = \varphi_{0_h}$$

where $\boldsymbol{u}_{0_h}$ and φ_{0_h} are suitable approximations of $\boldsymbol{u}_0$ and $\Gamma(0)$ respectively in $\boldsymbol{V}_h$ and Z_h.

The choice of $\boldsymbol{V}_h$ and Q_h depends on the fact this pair of space satisfies the so-called *inf-sup* condition

$$\inf_{\substack{q_h \in Q_h \\ q_h \neq 0}} \sup_{\substack{\boldsymbol{v}_h \in \boldsymbol{V}_h \\ \boldsymbol{v}_h \neq \boldsymbol{0}}} \frac{\int_\Omega \nabla \cdot \boldsymbol{v}_h q_h}{\|\boldsymbol{v}_h\|_{H^1(\Omega)} \|q_h\|_{L^2(\Omega)}} \geq \beta_h > 0 \qquad \forall h$$

and this condition ensures the existence and the uniqueness of the solution of the problem (36)-(37) as shown in [3]. In particular for our simulations we picked $r = 1$, whereas s is taken equal to 2.

3.1 Projection scheme for the Navier-Stokes equation

An intrinsic characteristic of the incompressible Naiver-Stokes equations is that velocity and pressure are coupled by the incompressibility constraint and we denote by *Standard* method the solution of the equations through a unique linear system.
The computational cost for solving the whole system is quite high: a common approach to overcome this issue is represented by the projection methods proposed for the first time by Chorin[1] and Temam[2]. Here we report a method similar to the one proposed in [15] that will be denoted as *ICT* (Incremental Chorin-Temam) method; first of all let us consider our discretized equations in a 'strong' form, where, unlike [15], we do not consider only the actual density in the time-derivative approximation but also the one associated to the previous iteration:

$$\frac{\rho(\varphi_h^{n+1})\boldsymbol{u}_h^{n+1} - \rho(\varphi_h^n)\boldsymbol{u}_h^n}{\Delta t} + \rho(\varphi_h^{n+1})\left(\boldsymbol{u}_h^n \cdot \nabla\right)\boldsymbol{u}_h^{n+1} - \frac{2}{Re}\nabla \cdot \left(\mu(\varphi_h^{n+1})\boldsymbol{D}(\boldsymbol{u}_h^{n+1})\right) + \nabla p_h^{n+1} = \boldsymbol{f}(\varphi_h^{n+1}) \quad (39)$$
$$\nabla \cdot \boldsymbol{u}_h^{n+1} = 0 \quad (40)$$

where $\boldsymbol{f} = -\frac{1}{Fr^2}\rho(\varphi_h^{n+1})\boldsymbol{e}_2 - \frac{1}{We}\nabla\cdot\left((\boldsymbol{I} - \boldsymbol{n}_\Gamma \otimes \boldsymbol{n}_\Gamma)\frac{dH_e}{d\varphi}\right)$ is the source term.

The main idea is to introduce an intermediate velocity $\widetilde{\boldsymbol{u}_h}^{n+1}$ that will satisfy the same boundary conditions of the original problem but will not be divergence free; moreover for what concerns the pressure we choose to compute it in an incremental way.

Hence we follow this procedure:

- **Step 1** Find $\widetilde{\boldsymbol{u}_h}^{n+1} \in \boldsymbol{V}$ such that

$$\frac{\rho(\varphi_h^{n+1})\widetilde{\boldsymbol{u}_h}^{n+1} - \rho(\varphi_h^n)\boldsymbol{u}_h^n}{\Delta t} + \rho(\varphi_h^{n+1})\left(\boldsymbol{u}_h^n \cdot \nabla\right)\widetilde{\boldsymbol{u}_h}^{n+1} - \frac{2}{Re}\nabla\cdot\left(\mu(\varphi_h^{n+1})\boldsymbol{D}(\widetilde{\boldsymbol{u}_h}^{n+1})\right) + \nabla p_h^n = \boldsymbol{f}(\varphi_h^{n+1}) \quad (41)$$

- **Step 2** Find $p_h^{n+1} \in Q$ such that

$$\frac{\rho(\varphi_h^{n+1})\boldsymbol{u}_h^{n+1} - \rho(\varphi_h^{n+1})\widetilde{\boldsymbol{u}_h}^{n+1}}{\Delta t} + \nabla\left(p_h^{n+1} - p_h^n\right) = 0$$

The previous equation can be rewritten as follows:

$$\frac{\boldsymbol{u}_h^{n+1} - \widetilde{\boldsymbol{u}_h}^{n+1}}{\Delta t} = -\frac{\nabla\delta p_h^{n+1}}{\rho(\varphi_h^{n+1})}$$

where $\delta p_h^{n+1} = p_h^{n+1} - p_h^n$. Taking the divergence of the above relation and, taking into account that $\nabla\cdot\boldsymbol{u}_h^{n+1}$ has to be equal to 0, we end up with the following equation:

$$\nabla\cdot\left(\frac{\nabla\delta p_h^{n+1}}{\rho(\varphi_h^{n+1})}\right) = \frac{1}{\Delta t}\nabla\cdot\widetilde{\boldsymbol{u_h}}^{n+1}$$

Since we want $\boldsymbol{u}_h^{n+1} \cdot \boldsymbol{n} = 0$ we are forced to consider the unphysical boundary condition

$$\nabla\delta p_h^{n+1} \cdot \boldsymbol{n} = 0$$

Hence the second step reads as follows: find $p_h^{n+1} \in Q$ such that

$$\begin{cases} \nabla\cdot\left(\frac{\nabla\delta p_h^{n+1}}{\rho(\varphi_h^{n+1})}\right) = \frac{1}{\Delta t}\nabla\cdot\widetilde{\boldsymbol{u_h}}^{n+1} \\ \nabla\delta p_h^{n+1} \cdot \boldsymbol{n} = 0 \end{cases} \quad (42)$$

- **Step 3**: We have now to project $\widetilde{\boldsymbol{u}_h}^{n+1}$ into the space of divergence-free functions

$$\boldsymbol{u}_h^{n+1} = \widetilde{\boldsymbol{u}_h}^{n+1} - \Delta t\frac{\nabla\delta p_h^{n+1}}{\rho(\varphi_h^{n+1})} \quad (43)$$

- **Step 4**: Finally we have to update the pressure

$$p_h^{n+1} = p_h^n + \delta p_h^{n+1} \quad (44)$$

17

The imposition on non-physical boundary conditions on the second step, which is an evidence of the splitting error induced by the projection method, is usually reflected in the appearance of some artificial boundary layer and can spoil a bit the accuracy of the method as explained in [14].

In general the scheme would be second-order accurate in velocity using the norm in $\boldsymbol{V}$ and in pressure using the norm in Q but, as it was mentioned before, the projection method is subjected to an intrinsic splitting error of order $\mathcal{O}(\Delta t)$ which prevents a full second-order accuracy.

Remark The second-order accuracy in time can be obtained using an A-stable second-order time stepping scheme, like BDF2.

Using a higher order scheme to approximate the time derivative operator is instead useless because of the irreducible splitting error that prevents any improvement [14].

3.2 Level-set discretization

At this point we can solve the equation for the advection of the level-set function. Since we are in presence of an hyperbolic type of equation, we need to add a stabilization term to (38) and two possibilities have been considered.

The first choice is the typical Streamline upwind Petrov-Galerkin (SUPG) scheme whose contribution to (38) reads as follows:

$$r = \int_{\Omega} \left(\frac{\varphi_h^{n+1} - \varphi_h^n}{\Delta t} + \boldsymbol{u}_h^n \cdot \nabla \varphi_h^{n+1} \right) \tau_K \boldsymbol{u}_h^n \cdot \nabla z_h d\Omega \tag{45}$$

with [21]:

$$\tau_K = \delta \frac{h_K}{\max \left(2 \left\| \boldsymbol{u}_h^n \right\|_{L^2(K)}, \frac{\text{tol}}{h_K} \right)}$$

where δ is a stabilization coefficient and $\frac{\text{tol}}{h_K}$ is introduced in order to avoid dividing by a number close to zero; for our simulations we picked $\delta = 0.01$, which is a good choice according to [21], and tol $= 10^{-3}$.

The convergence for linear transport equation can be proven in case the advection velocity does not depend on time[17], which is not the case. Anyway the scheme guarantees good results and it is a typical choice in the framework of stabilization[21]: this is also our pick throughout the numerical simulations unless otherwise specified.

The other choice is represented by the Interior Penalty (IP) method

$$\alpha \sum_{K \in \mathcal{T}_h} \int_{\partial K \backslash \partial \Omega} h_K^2 \left[\nabla \varphi_h^{n+1} \cdot \boldsymbol{n} \right] \left[\nabla z_h \cdot \boldsymbol{n} \right] dS \tag{46}$$

where α is the stabilization parameter.

3.3 Discretization for the reinitialization step

For what concerns the reconstruction step we use a Forward Euler discretization in order to keep the linearity; hence the discretization reads as follows:

$$\int_\Omega \frac{\varphi_h^{k+1} - \varphi_h^k}{\Delta\tau} z_h d\Omega - \int_\Omega \text{sign}_\gamma(\varphi_0)\left(1 - \left|\nabla\varphi_h^k\right|\right) z_h d\Omega + \beta \int_\Omega \nabla\varphi_h^k \cdot \nabla z_h d\Omega \quad \forall z_h \in Z_h \qquad (47)$$

with $\varphi_h^{k=0} = \varphi_0$.

Since we are interested in the steady state we stop in general when

$$\left\|\frac{\varphi_h^{k+1} - \varphi_h^k}{\Delta\tau}\right\|_{L^2(\Omega)} < \delta \qquad (48)$$

where δ is a prescribed tolerance.

It is worth to notice that we are not interested in reaching the solution $|\nabla\varphi| = 1$ along all the domain but only near the interface $\Gamma(t)$ and therefore a few iterations are in general sufficient for our purpose.

The time-step $\Delta\tau$ is sufficiently small in order to ensure the stability of the scheme, while γ and β are of order $\mathcal{O}(h)$.

In case the conservative level-set method is employed, the discretization reads as follows:

$$\int_\Omega \frac{\varphi_h^{k+1} - \varphi_h^k}{\Delta\tau} z_h d\Omega - \int_\Omega \left(\varphi_h^{k+1}(1 - \varphi_h^{k+1})\boldsymbol{n}_\Gamma\right) \cdot \nabla z_h d\Omega + \varepsilon \int_\Omega \left((\nabla\varphi_h^{k+1} \cdot \boldsymbol{n}_\Gamma)\boldsymbol{n}_\Gamma\right) \cdot \nabla z_h d\Omega = 0 \quad \forall z \in Z_h \quad (49)$$

with $\varphi_h^{k=0} = \varphi_0$.

In this case we chose an implicit treatment and we adopted the classical Newton method to solve numerically the equation. The stopping criterion remains (48) since also in this case we want to reach the steady-state.

It is important to keep ε as small as possible, since in [15] it has been shown that the analytical error evolves as:

$$A_{\varphi_h=0.5}(t^k) = A_{\varphi_h=0.5}(k=0) + \chi(t^k) \qquad (50)$$

where $A_{\varphi_h=0.5}$ is the area inside the 0.5 level set of φ_h and the following estimate holds for $\chi(t^k)$:

$$\left|\chi(t^k)\right| \leq 2L_\Gamma(t^k)\left|\kappa(t^k)\right|\varepsilon^2 \qquad (51)$$

with $L_\Gamma(t^k)$ denoting the perimeter of $\Gamma(t^k)$.

A common choice for $\Delta\tau$ and ε is represented by the pair

$$\Delta\tau = \frac{1}{2}h^{1+d}$$

$$\varepsilon = \frac{1}{2}h^{1-d}$$

with $0 < d < 1$. An appropriate choice is $d \approx 0.1$ [15].

19

4 Numerical simulations

In this section we present the results of the simulations of two traditional test-cases: the Rayleigh-Taylor instability and the rising bubble.
The implementation has been carried out in FEniCS through its Python interface.

4.1 Rayleigh-Taylor instability

The Rayleigh-Taylor instability occurs when the heavier fluid is above the lighter one: the horizontal interface between the two fluids becomes unstable and there is the formation of "fingers" inside the lighter fluid whose length growths in time.

For what concerns the adimensionalization we refer to [6] and therefore we take the reference length L equal to the computational width of the box W.
In the case of interfaces perturbed by a single wave, the wavelength may be the more relevant length; however, we choose W in order to be more flexible in the analysis since for interfaces perturbed by many different waves there is no a uniquely defined length-scale and W results the only length in common.
At this point the choice for the rest of the parameter is rather trivial since, as also reported in [6], the linear stability analysis shows that the time scale of wave growth is $\sqrt{\frac{W}{Ag}}$ where

$$A = \frac{\rho_2 - \rho_1}{\rho_2 + \rho_2}$$

is the Atwood number. Hence we end up with the following relations:

$$\boldsymbol{x} = W\boldsymbol{x}^* \qquad \boldsymbol{u} = \sqrt{AgW}\boldsymbol{u}^* \qquad t = \sqrt{\frac{W}{Ag}}t^*$$

Moreover we choose for this problem as reference density and viscosity the ones associated to the lighter fluid and therefore we obtain:

$$\rho = \rho_1\rho^* \qquad \mu = \mu_1\mu^* \qquad Re = \frac{\rho_1 L\sqrt{AgL}}{\mu_1} \qquad Fr = \sqrt{A} \qquad We = \frac{\rho_1 AgL^2}{\sigma} = A \cdot Bo$$

where

$$Bo = \frac{\rho_1 gL^2}{\sigma}$$

is the Bond number[22].

It is worthwhile to rewrite (16) taking into account the non-dimensional parameters just computed above:

$$\rho\left(\frac{\partial \boldsymbol{u}}{\partial t} + (\boldsymbol{u} \cdot \nabla)\boldsymbol{u}\right) - \frac{1}{Re}\nabla\cdot(2\mu\boldsymbol{D}(\boldsymbol{u})) + \nabla p = -\frac{1}{A}\rho\boldsymbol{e}_2 - \frac{1}{A}\frac{1}{Bo}\kappa\boldsymbol{n}_\Gamma\delta(\Gamma) \qquad (52)$$

where we clearly omitted the $(\cdot)^*$ symbol to indicate non-dimensional quantities.

The computational domain is the rectangle $(0, W) \times (0, 4W)$ with $W = 1\,\text{m}$; for what concerns the mesh we consider a 64 x 256 partition as reported in [10].
Eventually we choose not to consider the surface tension effects, namely we set $\sigma = 0$.
The fluid is at rest at $t = 0$, while the initial position of the perturbed interface is taken equal to

$$\varphi(\boldsymbol{x}, 0) = y - 2W - 0.04W \cos(2\pi x)$$

The Reynolds number is set equal to 156.6, the Atwood number is taken equal to 0.6667 and the viscosity ratio $\frac{\mu_2}{\mu_1} = 10$ in analogy to [13].
In the code we implemented the possibility to impose directly the value of the non-dimensional parameters

```python
#Compute the Atwood number and the Reynolds number according to how the
    settings has been imposed
        if(self.set_type == 'Physical'):
            try:
                self.rho1 = float(self.Param["Lighter_density"])
                self.rho2 = float(self.Param["Heavier_density"])
                self.At = (self.rho2 - self.rho1)/(self.rho2 + self.rho1)
                if(self.rho2 < self.rho1 and self.rank == 0):
                    warnings.warn("The heavier density is not greater than the
                        lighter one")
                self.Re =
                    self.rho1*self.L0*np.sqrt(self.At*self.L0*self.g)/self.mu1
                assert self.Re > 1.0, "Invalid Reynolds number computed"
            except RuntimeError as e:
                if(self.rank == 0):
                    print(str(e) + "\nPlease check configuration file")
                exit(1)
        elif(self.set_type == 'Parameters'):
            try:
                self.At = float(self.Param["Atwood_number"])
                if(self.At < 0.0 or self.At > 1.0):
                    raise ValueError("Invalid Atwood number")
                self.Re = float(self.Param["Reynolds_number"])
                if(self.Re < 1.0):
                    raise ValueError("Invalid Reynolds number")
                self.rho1 =
                    self.Re*self.mu1/(self.L0*np.sqrt(self.At*self.L0*self.g))
                self.rho2 = self.rho1*(1.0 + self.At)/(1.0 - self.At)
            except RuntimeError as e:
                if(self.rank == 0):
                    print(str(e) + "\nPlease check configuration file")
                exit(1)
```

Finally, a no-slip condition $\boldsymbol{u} = \boldsymbol{0}$ is enforced at the bottom and top walls, while on the two vertical sides the first component of velocity (the normal one) is imposed equal to 0, and we take the interface thickness $\varepsilon = 0.05$.

We choose to employ the non-conservative version of the level-set method with the reinitialization equation (18) because it is more convenient from a computational point of view due to the linearity of all the steps.
We point out here a fact related to the reinitialization approach that holds in any situation and that we have already mentioned: the achievement of the steady-state is not really necessary since the recovery of the signed-distance function property is important only nearly the interface rather than over the entire domain; hence, since we start from a function that is close to satisfy the property we desire, a few iterations are sufficient to reach our goal and this number is typically chosen empirically: in our case we set a maximum number of 10 sub-iterations for the reinitialization step.

Let us show now the results obtained:

(a) Standard method   (b) ICT method
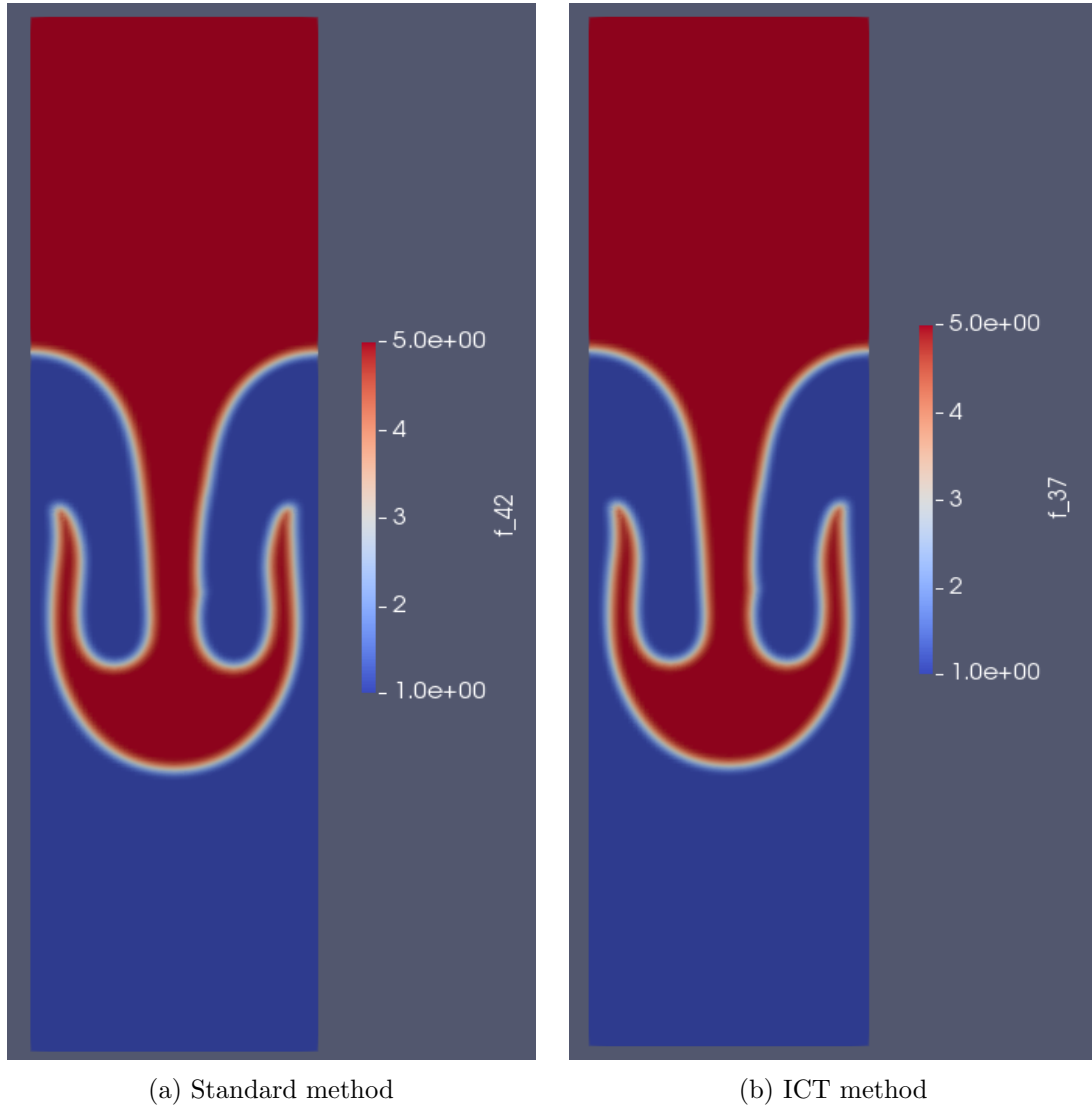
Figure 2: Rayleigh-Taylor instability at $t = 1.2\,\mathrm{s}$

First of all we notice that the projection scheme proposed seems to work quite well since
we do not see significant differences in the obtained results.

We are able to catch the main behaviour of the Rayleigh-Taylor instability: as the heavier
fluid penetrates the light fluid, the interface begins to roll up along the sides of the spike
giving the typical "mushroom" shape.

(a) Standard method　　　　　　　　　　　　　　(b) ICT method
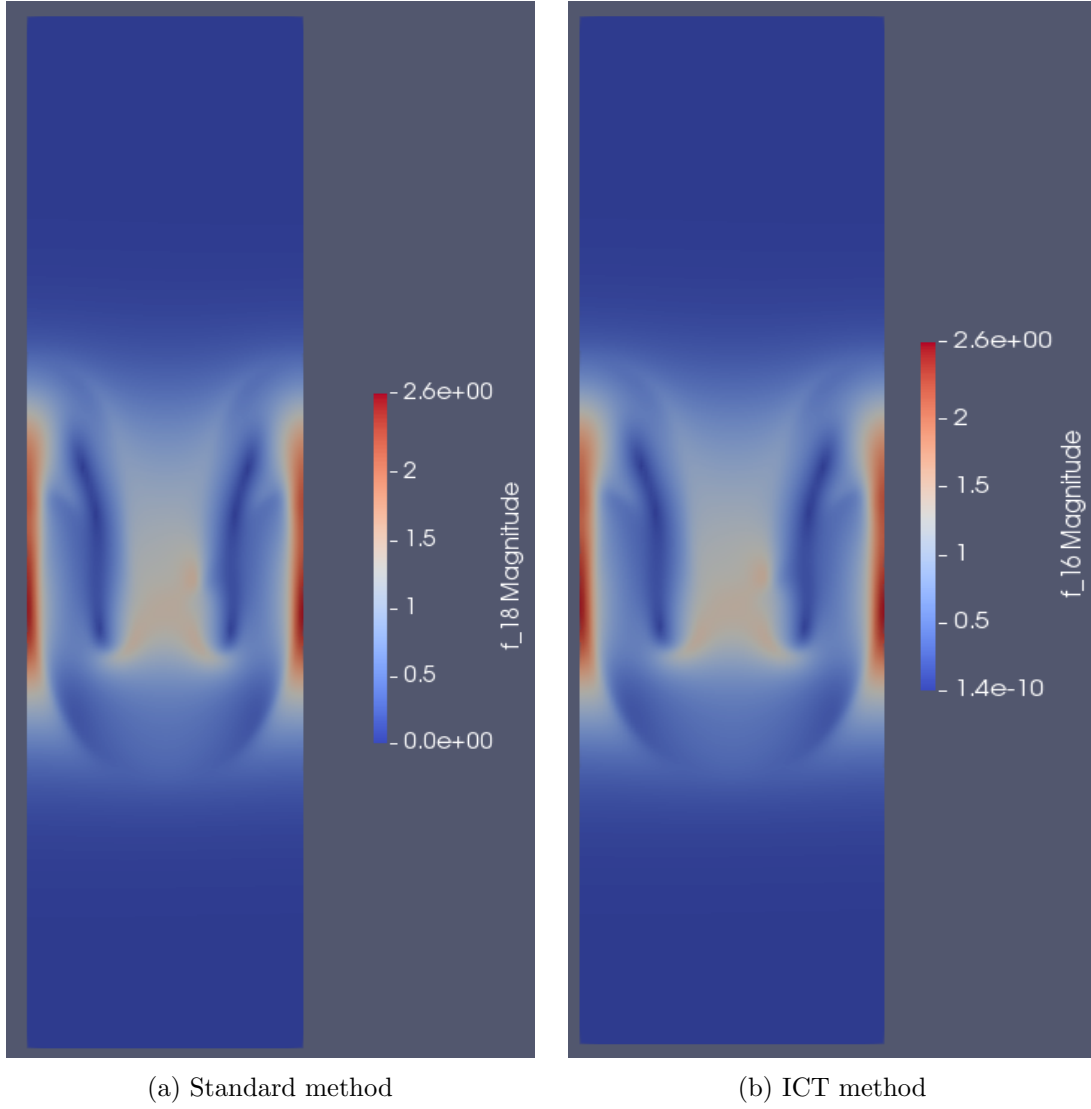
Figure 3: Velocity magnitude at $t = 1.2\,\mathrm{s}$

Eventually we notice from the picture above that the boundary condition is well imposed also in the ICT method with an error of the order of 10^{-10} with respect to the Standard method.

An interesting analysis regards the influence of the Atwood number; in order to make this study we fix the Reynolds ($Re = 100$) and we vary the Atwood number ($A = 0.3, A = 0.4, A = 0.5$).
Inspired by [23], we consider for this analysis the following expression for the initial

interface:

$$\varphi(\boldsymbol{x}, 0) = \tanh \frac{y - 2W - 0.1 \cos(2\pi x)}{0.01\sqrt{2}}$$

(a) $A = 0.3$ (b) $A = 0.4$ (c) $A = 0.5$
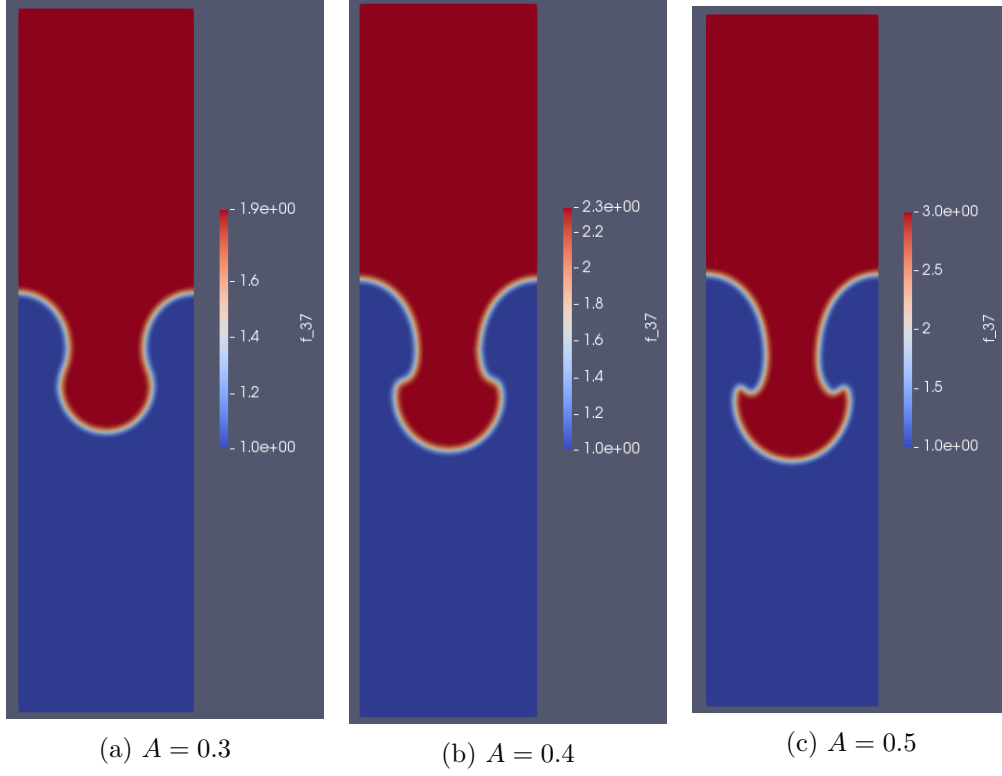
Figure 4: Shape comparison at $t = 0.8\,\mathrm{s}$ $(Re = 100)$

It can be easily seen from the figure above that with increasing Atwood number the mushroom is more roll up; this points out the earlier appearance of the Kelvin-Helmotz instability which is due to the development of short wavelength perturbations along the fluid interface.

4.2 Two-dimensional rising bubble

The next application is a circular bubble rising in a viscous fluid.
This benchmark has been intensively studied in [16] and we refer to it in order to choose an adequate setting.

The initial configuration consists of a fluid at rest with interface $\Gamma(0)$ represented by a circular bubble of radius $r_0 = 0.25$ centered in $(0.5; 0.5)$ in the rectangular domain $(0,1) \times (0,2)$, hence:

$$\varphi(\boldsymbol{x}, 0) = \sqrt{(x-0.5)^2 + (y-0.5)^2} - 0.25$$

The no-slip condition is set at the top and bottom boundaries, while the free-slip condition is imposed on the vertical walls. The density of the bubble is smaller than the one of the surrounding fluid.
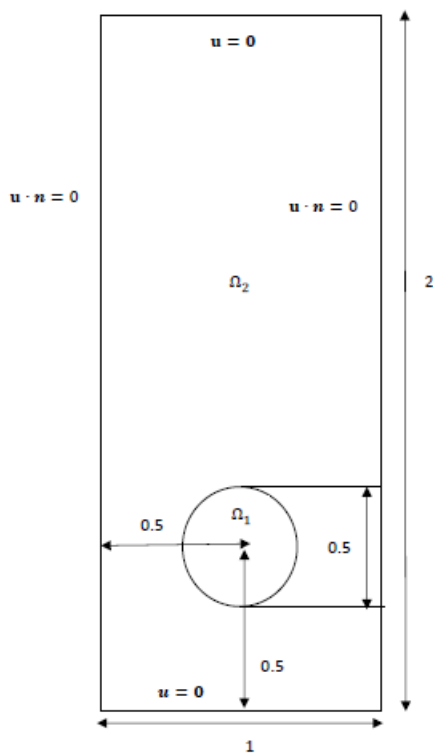
Figure 5: Initial and boundary conditions for the rising bubble

For what concerns the non-dimensionalization, a natural choice for the reference length is the diameter $2r_0$, while for the reference velocity we take the gravitational velocity $\sqrt{2gr_0}$. Therefore we obtain

$$Re = \frac{\rho_2 L\sqrt{gL}}{\mu_2} \qquad Fr = 1 \qquad We = \frac{\rho_2 g L^2}{\sigma} = Bo$$

where the reference density and viscosity are associated to the heavier fluid.

We report now the physical parameters that will be employed throughout our simulations:

ρ_1	ρ_2	μ_1	μ_2	g	σ	ε	Re	Bo	ρ_2/ρ_1	μ_2/μ_1
1	1000	0.1	10	0.98	1.96	0.025	35	125	1000	100

For what concerns the computational mesh we consider a reference size $h = \frac{1}{80}$ and therefore we end up with a 80×160 grid, while the time-step is taken equal to $\frac{h}{16} = 0.0008$ and the final time is $T_f = 3$, exactly like in [16].
Eventually, we choose to employ the ICT method that showed good performances in the previous benchmark and is computationally cheaper. The solution of the linear systems relies on GMRES iterative solver with "default" preconditioner.

```
self.solver_Levset = "gmres"
self.precon_Levset = "default"
self.solver_recon = "gmres"
self.precon_recon = "default"
...
self.solver_ICT_1 = "gmres"
self.precon_ICT_1 = "default"
self.solver_ICT_2 = "gmres"
self.precon_ICT_2 = "default"
self.solver_ICT_3 = "gmres"
self.precon_ICT_3 = "default"
```

The first comparison regards the two level-set methods presented in the previous sections: the classical one (with interface thickness $\varepsilon = 0.025$) and the conservative one.

(a) Classical level-set   (b) Conservative level-set
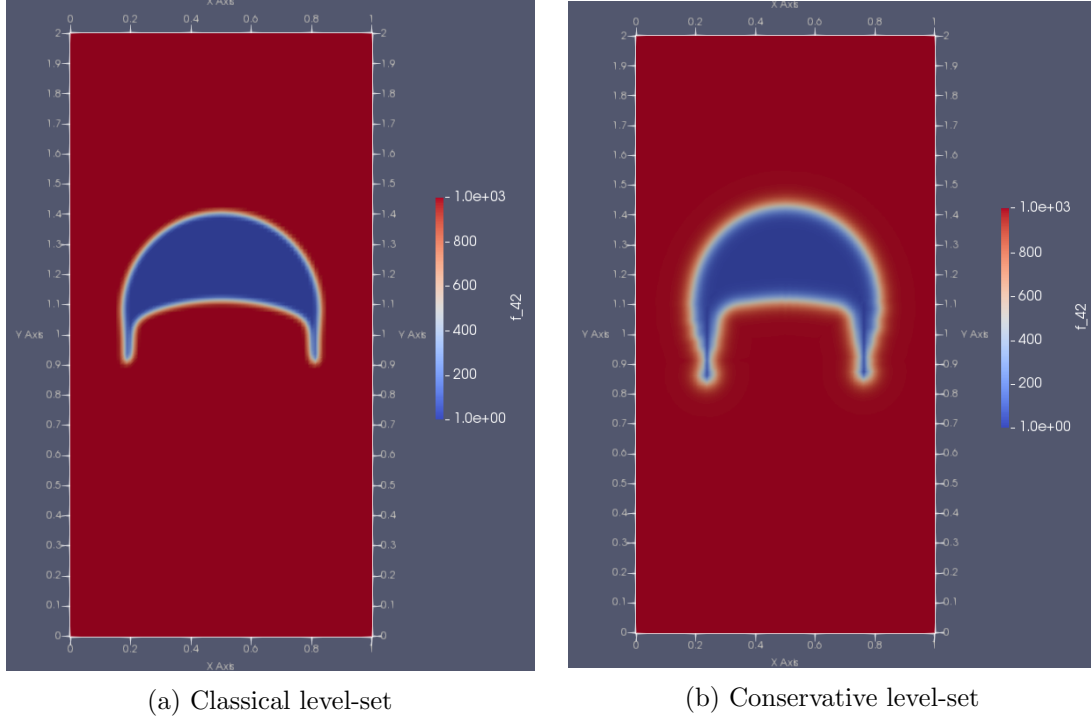
Figure 6: Bubble shape at $t = 3\,\mathrm{s}$

The shapes at the final time are similar from a qualitative point of view and also the height reached by the bubble is analogous between the two simulations.

In order to decide which method is more appropriate we compute the area of the bubble; indeed, since the fluid is considered incompressible, we should find a conservation of the area during the whole time evolution.

The computation of the area is different between the two cases: in case of classical level-set method

$$|\Omega_1(t)| = \int_{\Omega_1(t)} d\Omega = \int_\Omega \mathbb{1}_{\{\varphi(\boldsymbol{x},t)<0\}} d\Omega \tag{53}$$

where $\mathbb{1}_{\{\cdot\}}$ is the indicator function of the set $(\cdot)$.

On the other hand in case of conservative level-set we need to apply the following relation:

$$|\Omega_1(t)| = \int_{\Omega_1(t)} d\Omega = \int_\Omega \mathbb{1}_{\left\{\varphi(\boldsymbol{x},t)<\frac{1}{2}\right\}} d\Omega \tag{54}$$

28
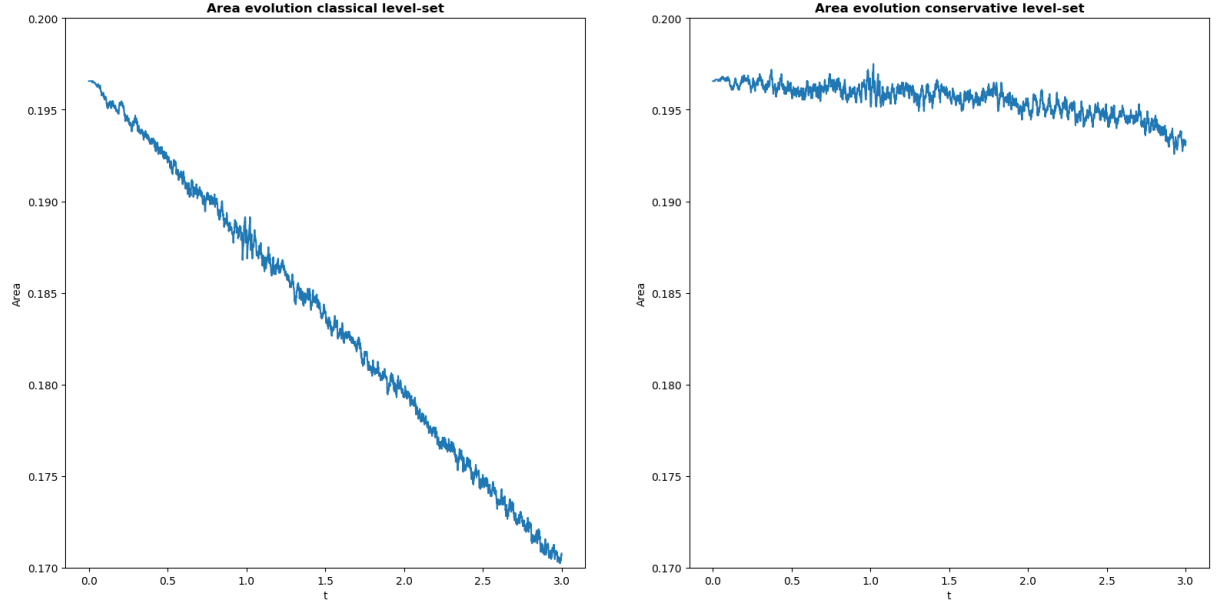
Figure 7: Time evolution of bubble area

The lack of mass related to the classical level-set method is very important, whereas the results obtained with the conservative method are really satisfactory with only a little more than 1% of mass lost:

$$|\Omega_1(0)| = 0.19635$$
$$|\Omega_1(3)| = 0.1933$$

Moreover most of the volume loss occurs towards the end of the computation where our regime is near a break-up as explained in [16].
Hence we decide to examine in depth the conservative level-set method.

At this point we ask ourselves if it is really necessary to apply the reinitialization procedure at every increment of time; indeed this step, which is fundamental to guarantee the accuracy of the results, is however characterized by a lack of mass of the order of ε^2 at each time as evident from (51).
In order to perform this test we decide to solve (23) every 5, 10, 20 and 40 time steps and we compare the evolution of the area in the different cases.
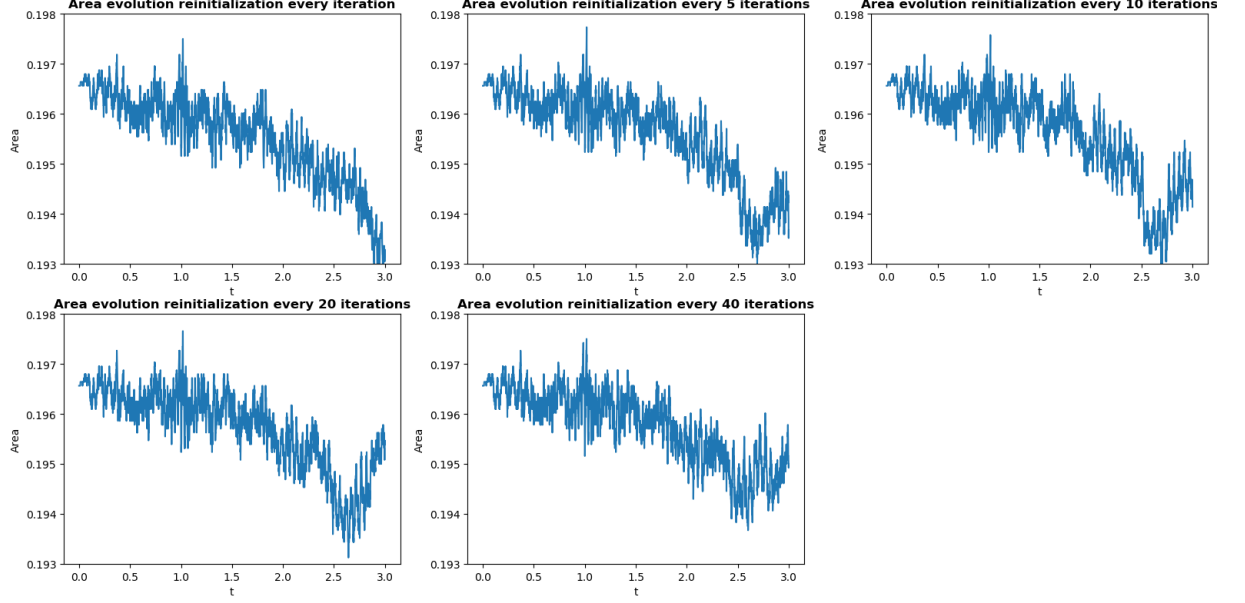
Figure 8: Comparison of area for the reinitialization step

From the picture above we do not notice many differences between the various instances, or rather, the mass loss seems to be reduced in the latter case when reinitialization is applied more rarely.

Nevertheless when we try to perform the reinitialization procedure every 80 time steps, we are not able to reach convergence; this suggests us that the shape of the bubble is not well caught when reinitialization is not applied sufficiently often.

We verify this hypothesis computing the *degree of circularity*[16] which is defined as:

$$\chi(t) = \frac{P_a(t)}{P_b(t)} = \frac{\text{perimeter of the area-equivalent circle}}{\text{perimeter of the bubble}} \tag{55}$$

Here P_a denotes the perimeter of a circle with the same area of the bubble, whereas P_b is the actual perimeter. For a perfectly circular bubble, the circularity is equal to 1 and then decrease as the object is deformed. The value P_b is computed as follows:

$$P_b(t) = \int_{\Gamma(t)} d\Sigma = \int_{\Omega} \delta(\Gamma(t))d\Omega = \int_{\Omega} \delta(\varphi) \, |\nabla\varphi| \, d\Omega \approx \int_{\Omega} \delta_\varepsilon(\varphi) \, |\nabla\varphi| \, d\Omega = \int_{\Omega} |\nabla\varphi| \, d\Omega \tag{56}$$

```
if(self.reinit_method == 'Conservative'):
    Vol = assemble(conditional(lt(self.phi_old, 0.5), 1.0, 0.0)*dx)
    Pa = 2.0*sqrt(np.pi*Vol)
    Pb = assemble(mgrad(self.phi_old)*self.Appr_Delta(self.phi_old,self.eps)*dx)
    Chi = Pa/Pb
    ...
elif(self.reinit_method == 'Non_Conservative_Hyperbolic'):
```

```
Vol = assemble(conditional(lt(self.phi_old, 0.0), 1.0, 0.0)*dx)
Pa = 2.0*sqrt(np.pi*Vol)
Pb = assemble(mgrad(self.phi_old)*self.Appr_Delta(self.phi_old,self.eps)*dx)
Chi = Pa/Pb
```
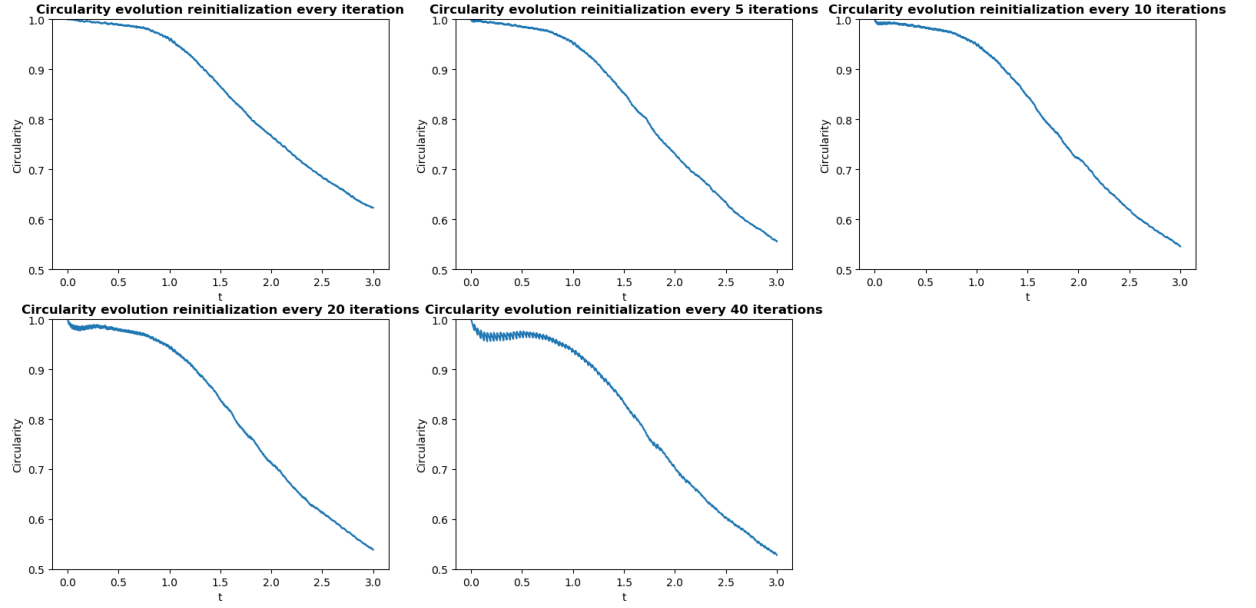

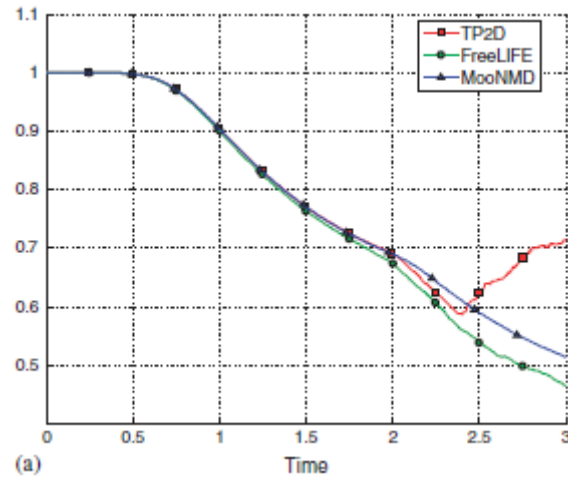Figure 9: Comparison of circularity for the reinitialization step


Figure 10: Circularity evolution in [16]

31

If we compare the results of our simulations with the ones in [16], we see a good agreement between the data, in particular with the computations performed using MooNMD. The analysis of the circularity shows that there are some spurious oscillations at the beginning when we perform the reinitialization procedure every 20 time steps and, above all, 40 time steps.

Therefore we pick 10 time steps as reference value for which applying the reinitialization step: this seems to be a good trade-off between computational cost and accuracy.

For the sake of curiosity we report here the bubble shape at final time under the conditions just mentioned and we compare it with the results in [16]
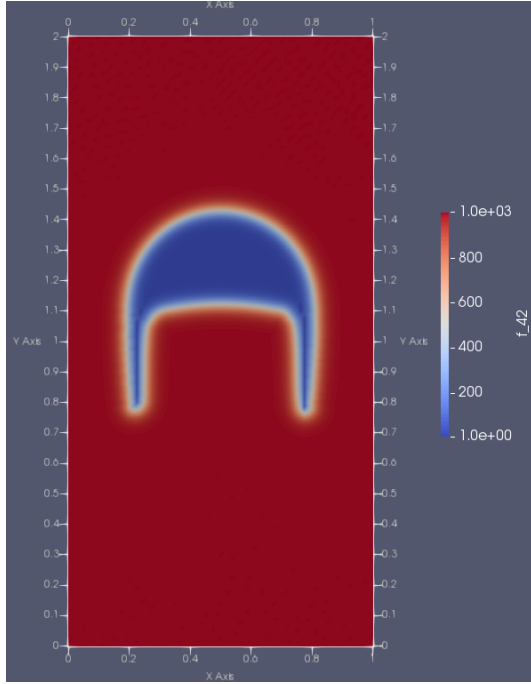
(a) Our simulation: reinitialization every 10 iterations
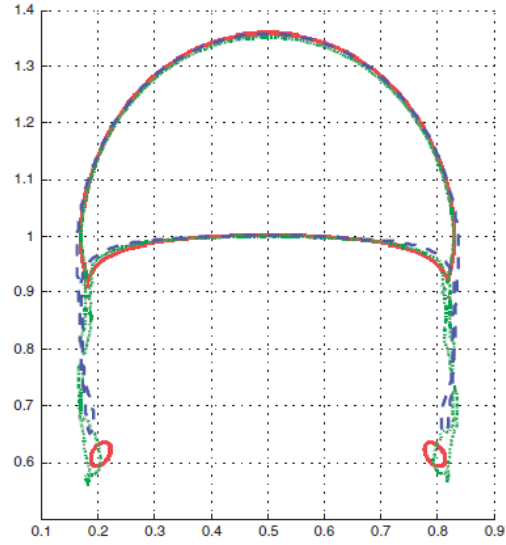
(b) Bubble shape in [16]: TP2D (solid red), FreeLIFE (dotted green) and MooNMD (dashed blue)

Figure 11: Bubble shape comparison at t = 3 s

We notice a very similar behaviour in the final shape especially with the MooNMD simulation again; the only significant difference is in the height reached by the bubble that is slightly greater in our simulation rather than the one in [16].

Other two benchmark quantities computed in [16] are the centroid of the center of

mass $\boldsymbol{X}_c$ and the rising velocity $\boldsymbol{U}_c$ respectively defined as:

$$\boldsymbol{X}_c = (x_c, y_c) = \frac{\int_{\Omega_1} \boldsymbol{x}\, d\Omega}{\int_{\Omega_1} d\Omega} \tag{57}$$

$$\boldsymbol{U}_c = (u_c, v_c) = \frac{\int_{\Omega_1} \boldsymbol{u}\, d\Omega}{\int_{\Omega_1} d\Omega} \tag{58}$$

(a) Our simulation

(b) Results from [16]
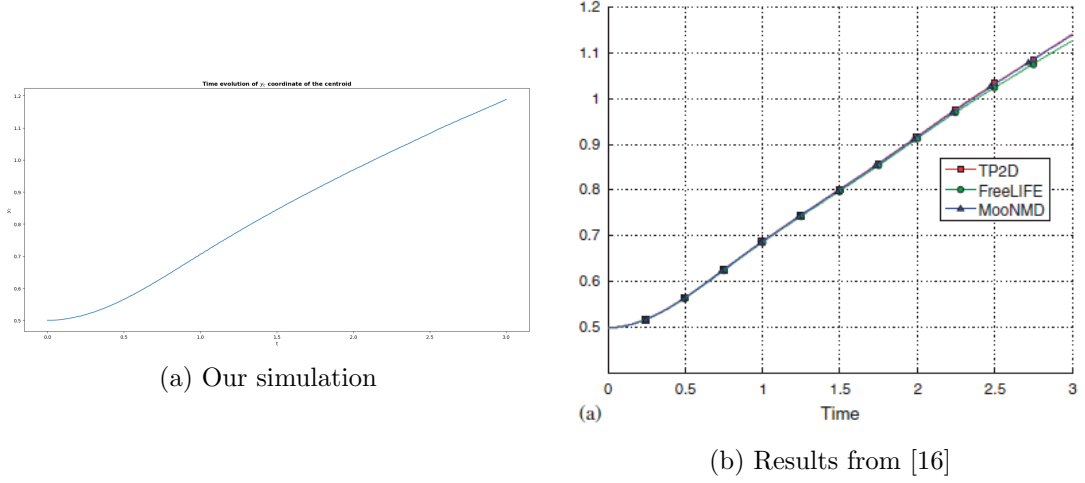
Figure 12: Comparison of y_c time evolution

(a) Our simulation

(b) Results from [16]
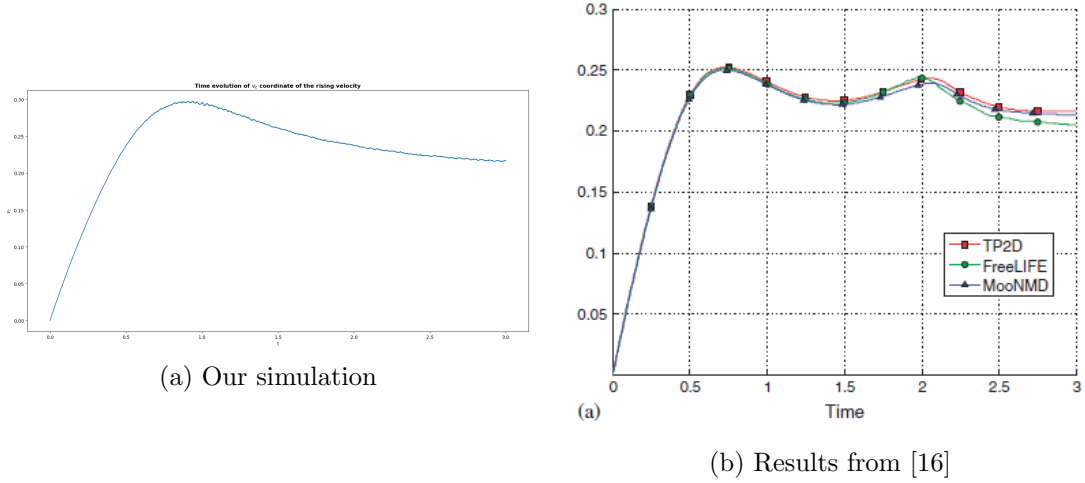
Figure 13: Comparison of v_c time evolution

The comparison from the pictures above confirm the fact that we obtained slightly higher values in our simulations, but the overall behaviour is well caught, especially for the centroid.

33
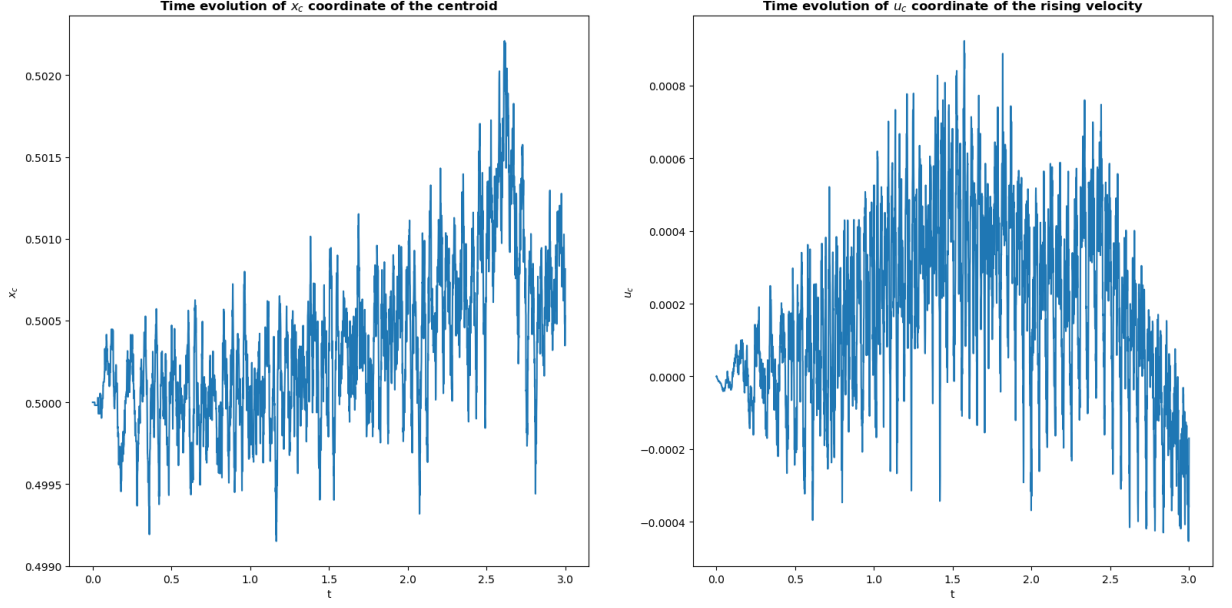
Figure 14: Time sequence of x_c and u_c

Using x_c and u_c we observe the symmetry in the motion of the bubble: denote by $\overline{x_c}$ the time average of x_c and by $\overline{u_c}$ the time average of u_c:

$$\overline{x_c} = 0.50034 \implies |\overline{x_c} - x_c(0)| = 3.4 \cdot 10^{-4}$$
$$\overline{u_c} = 1.7731 \cdot 10^{-4} \implies |\overline{u_c} - u_c(0)| = 1.7731 \cdot 10^{-4}$$

which result to be small values compared to what happens in the other direction.

Finally, we perform an analysis on the grid resolution by comparing the time evolution of the area, of y_c and of u_c. It is important to notice that in the various simulations we fix the time-step as $\frac{h}{16}$ exactly as we did so far.
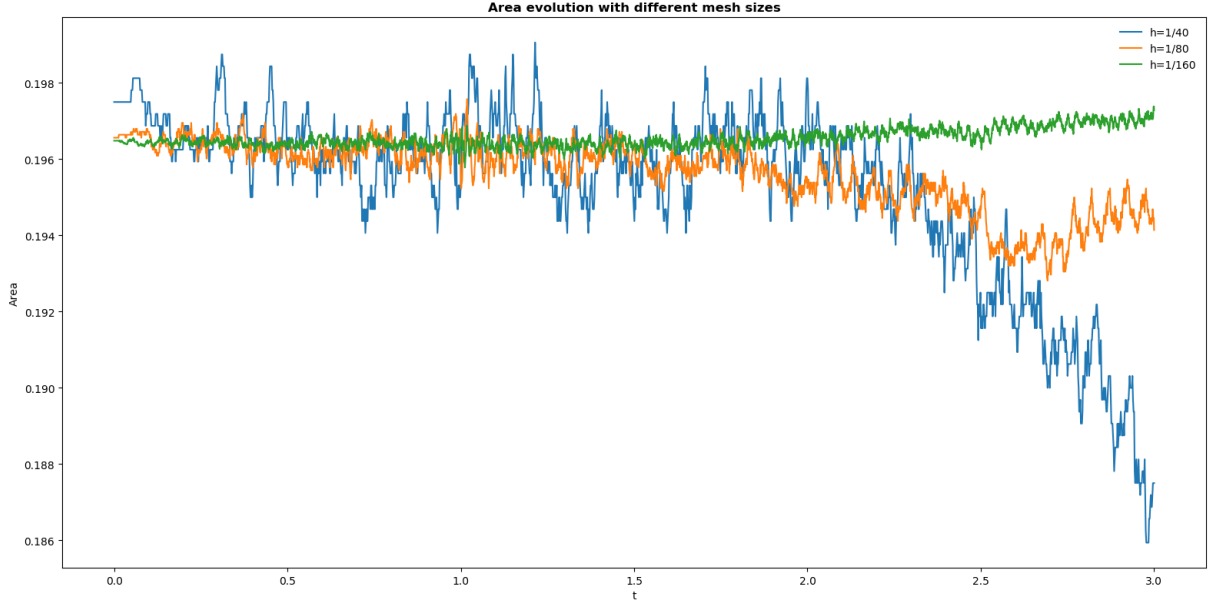
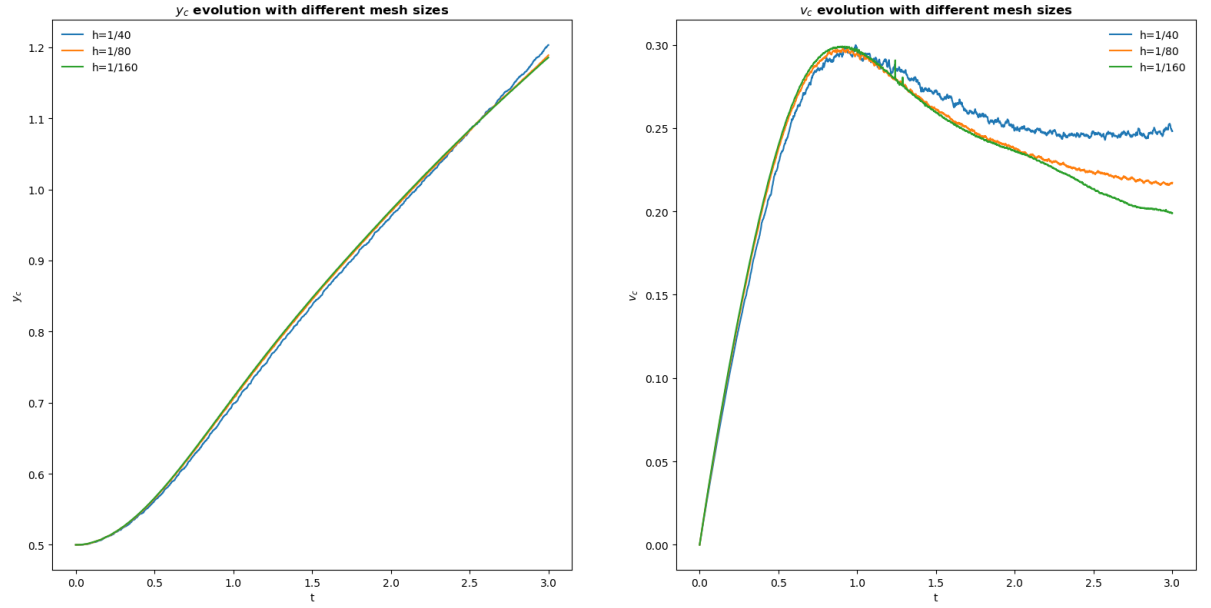Figure 15: Time evolution of area with different h

Figure 16: Time evolution of y_c and v_c with different h

The results obtained are in agreement with what is reported in [16]: we need a certain resolution in order to guarantee the mass conservation and clearly things go better as the mesh size decreases.

The vertical position of the center of mass converges well toward the solution obtained

35

with the finest grid, whereas a very good agreement can be seen for the curve describing the vertical component of the rising velocity up to the maximum. From then on the curve corresponding to the simulation performed on the coarsest shows some spurious oscillations, while the other two keep in contact until we approach the end of the simulation where we see some irregularities (especially in the simulation where $h = \frac{1}{80}$) probably due to the deformation and to some oscillations in the velocity field near the interface.

For the sake of completeness we report here the results obtained using the IP stabilization with a value of the stabilization parameter α equal to 0.1
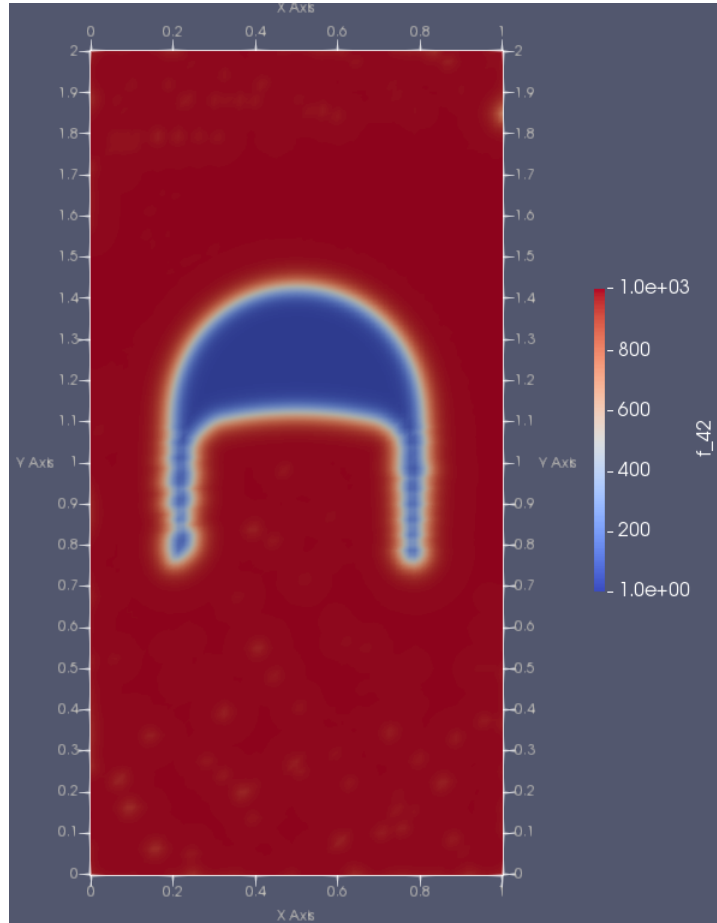

Figure 17: Bubble shape at $t = 3$ s using IP stabilization

The results are less satisfactory with respect to the one obtained employing SUPG: the interface is not perfectly symmetric and we notice the presence of some spurious oscillations.
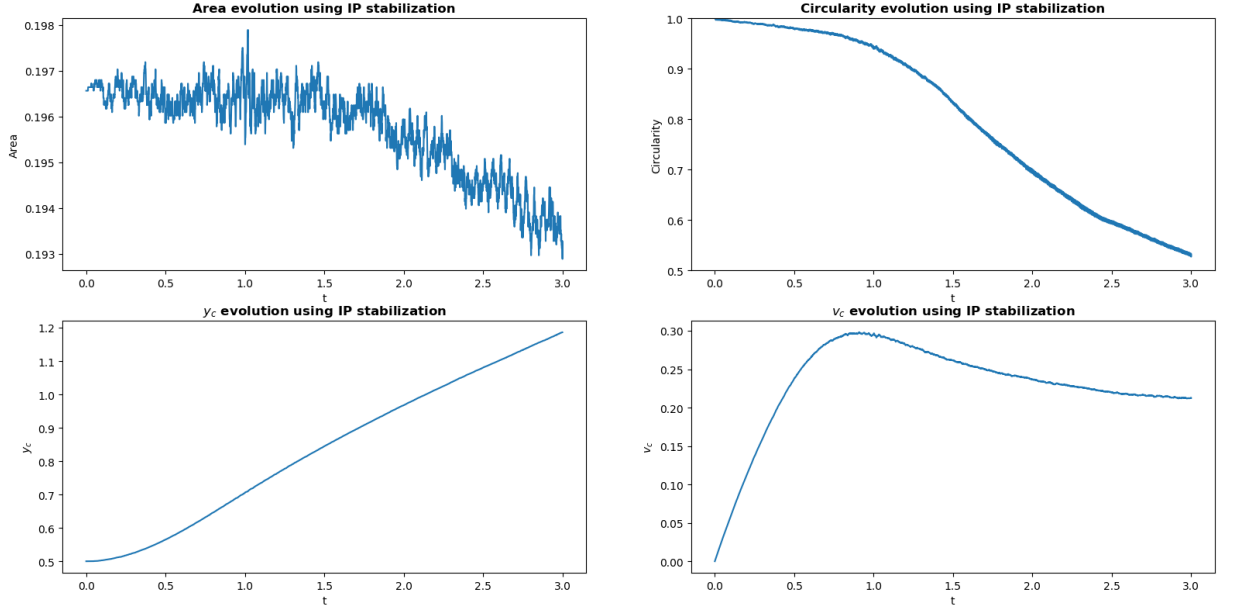
Figure 18: Benchmark quantities using IP stabilization

Nevertheless the evolution of the benchmark quantities employed above (area, degree of circularity, vertical components of the centroid and of the rising velocity) is very similar to the one obtained using SUPG.

References

[1] Chorin A. "Numerical Solution of the Navier-Stokes Equations". In: *Mathematics of Computation* 22 (1968), pp. 745–762. DOI: 10.2307/2004575.

[2] Temam R. "Sur l'approximation de la solution des equationes par la methode de pas fractionnaires ii". In: *Arch. Ration. Mech. Anal. 33* (1969), pp. 377–385.

[3] Girault V. and Raviart P. A. *Finite Element Approximation of the Navier-Stokes Equations, Lecture Notes in Mathematics*. Springer-Verlag, 1979.

[4] Estrada R. and Kanwal R. P. "Applications of Distributional Derivatives to Wave Propagation". In: *IMA Journal of Applied Mathematics* 26.1 (1980), pp. 39–63. ISSN: 0272-4960. DOI: 10.1093/imamat/26.1.39.

[5] Estrada R. and Kanwal R. P. "Distributional Analysis for Discontinuous Fields". In: *Journal of Mathematical Analysis and Applications* 105 (1985), pp. 478–490.

[6] Tryggvason G. "Numerical simulations of the Rayleigh-Taylor instability". In: *Journal of Computational Physics* 75.2 (1988), pp. 253–282. ISSN: 0021-9991. DOI: https://doi.org/10.1016/0021-9991(88)90112-X.

[7] Diperna R. J. and Lions P. L. "Ordinary differential equations, transport theory and Sobolev spaces". In: *Inventiones mathematicae* 98 (1989), pp. 511–547.

[8] Brackbill J. U., Kothe D.B, and Zemach C. "A continuum method for modeling surface tension". In: *Journal of Computational Physics* 100.2 (1992), pp. 335–354. ISSN: 0021-9991. DOI: https://doi.org/10.1016/0021-9991(92)90240-Y.

[9] Sussman M., Smereka P., and Osher S. "A Level Set Approach for Computing Solutions to Incompressible Two-Phase Flow". In: *Journal of Computational Physics* 114.1 (1994), pp. 146–159. ISSN: 0021-9991. DOI: https://doi.org/10.1006/jcph.1994.1155.

[10] Puckett E. G. et al. "A High-Order Projection Method for Tracking Fluid Interfaces in Variable Density Incompressible Flows". In: *Journal of Computational Physics* 130.2 (1997), pp. 269–282. ISSN: 0021-9991. DOI: https://doi.org/10.1006/jcph.1996.5590.

[11] Fedkin R. and Osher S. *The Level Set Methods and Dynamic Implicit Surfaces*. Springer Nature, 2003.

[12] Olsson E. and Kreiss G. "A conservative level set method for two phase flow". In: *Journal of Computational Physics* 210.1 (2005), pp. 225–246. ISSN: 0021-9991. DOI: https://doi.org/10.1016/j.jcp.2005.04.007.

[13] Salih A. and Ghosh Moulic S. "Simulation of Rayleigh-Taylor Instability Using Level Set Method". In: 2006.

[14] Guermond J.L., Minev P., and Shen J. "An overview of projection methods for incompressible flows". In: *Computer Methods in Applied Mechanics and Engineering* 195 (Sept. 2006), pp. 6011–6045. DOI: 10.1016/j.cma.2005.10.010.

[15] Olsson E., Kreiss G, and Zahedi S. "A conservative level set method for two phase flow II". In: *Journal of Computational Physics* 225.1 (2007), pp. 785–807. ISSN: 0021-9991. DOI: https://doi.org/10.1016/j.jcp.2006.12.027.

[16] Hysing S. et al. "Quantitative benchmark computations of two-dimensional bubble dynamics". In: *International Journal for Numerical Methods in Fluids* 60 (2009), pp. 1259–1288. DOI: 10.1002/fld.1934.

[17] Burman E. "Consistent SUPG-method for transient transport problems: Stability and convergence". In: *Computer Methods in Applied Mechanics and Engineering* 199 (Mar. 2010), pp. 1114–1123. DOI: 10.1016/j.cma.2009.11.023.

[18] Johansson N. "Implementation of a standard level set method for incompressible two-phase flow simulations". In: 2011.

[19] Zahedi S. "Numerical Methods for Fluid Interface Problems". In: 2011.

[20] Quarteroni A. *Modellistica numerica per problemi differenziali*. Vol. 5. Springer-Verlag, 2012.

[21] Loch E. and Reusken A. "The level set method for capturing interfaces with applications in two-phase flow problems". In: 2013.

[22] Rapp B. E. "Chapter 9 - Fluids". In: *Microfluidics: Modelling, Mechanics and Mathematics*. Ed. by Bastian E. Rapp. Micro and Nano Technologies. Oxford: Elsevier, 2017, pp. 243–263. ISBN: 978-1-4557-3141-1. DOI: https://doi.org/10.1016/B978-1-4557-3141-1.50009-5.

[23] Khan S. and Shah A. "Simulation of the two-dimensional Rayleigh-Taylor instability problem by using diffuse-interface model". In: *AIP Advances* 9 (Aug. 2019), p. 085312. DOI: 10.1063/1.5100791.